# River bank erosion and lateral accretion linked to hydrograph recession and flood duration in a mountainous snowmelt-dominated system

**Nicholas A. Sutfin[1*], Joel C. Rowland[1], Mulu Fratkin[1], Sophie Stauffer[1], Rosemary W.H. Carroll[2], Wendy Brown[3], Kenneth H. Williams[3,4]**

[1]Earth and Environmental Sciences Division, Los Alamos National Laboratory, Los Alamos, NM

[2]Division of Hydrologic Sciences, Desert Research Institute, Reno, NV

[3]Rocky Mountain Biological Laboratory, Gothic, CO

[4]Lawrence Berkeley National Laboratory, Berkeley, CA

***** Current affiliation: Dept. of Earth, Environmental, and Planetary Sciences, Case Western Reserve University, Cleveland, OH

Corresponding authors: Nicholas A. Sutfin (Nicholas.sutfin@case.edu), Joel Rowland (jrowland@lanl.gov)

**Key Points:**

- Floodplain erosion and accretion estimated over 60 years using aerial lidar, repeat aerial imagery, field surveys, and historic flow data
- Recession limb slope, flow duration, channel width, and sinuosity were significantly linked to lateral erosion and accretion in 9 reaches
- Hydrograph recession and flood duration explain 91% and 59% of variability in bank erosion and accretion along an 11-km study segment

## Abstract

Changes in the magnitude and frequency of river flows have potential to alter sediment dynamics and morphology of rivers globally, but the direction of these changes remains uncertain. A lack of data across spatial and temporal scales limits understanding of river flow regimes and how changes in these regimes interact with river bank erosion and floodplain deposition. Linking characteristics of the flow regime to changes in bank erosion and floodplain deposition is necessary to understand how rivers will adjust to changes in hydrology from societal pressures and climatic change, particularly in snowmelt-dominated systems. We present a lidar dataset, intensive field surveys, aerial imagery and hydrologic analysis spanning 60 years, and spatial analysis to quantify bank erosion, lateral accretion, floodplain overbank deposition, and a floodplain fine sediment budget in an 11-km long study segment of the meandering gravel bed East River, Colorado, USA. Stepwise regression analysis of channel morphometry in nine study reaches and snowmelt-dominated annual hydrologic indices in this mountainous system suggest that sinuosity, channel width, recession slope, and flow duration are linked to lateral erosion and accretion. The duration of flow exceeding baseflow and the slope of the annual recession limb explain 59% and 91% of the variability in lateral accretion and erosion, respectively. This strong correlation between the rate of change in river flows, which occurs over days to weeks, and erosion suggests a high sensitivity of sedimentation along rivers in response to a shifting climate in snowmelt-dominated systems, which constitute the majority of rivers above 40° latitude.

## Plain Language Summary

Changing climatic conditions are poised to alter the timing and magnitude of precipitation, snowpack, snowmelt and the balance of water and sediment within river corridors. Understanding how these changes affect the stability of land along rivers is important for securing infrastructure, maintaining healthy ecosystems, preserving water quality, and understanding the fate and transport of contaminated sediment. This research uses aerial imagery, laser topographic scanning technology, field measurements of water and soil, and historical river flow data to examine linkages between river flows and erosion and deposition of sediment along the floodplain of a mountain river over 60 years. Results show that river bank erosion is linked to the rate at which the river flows decrease following snowmelt-driven peaks and that the amount of sediment that is deposited along the river banks is linked to the duration of flooding. These results have important implications for understanding how rivers and freshwater resources may be impacted by shifting climatic conditions and hydrologic regimes.

## 1 Introduction

A large number of studies have quantified long-term channel migration and episodic bank erosion, but have been limited in the examination of the link between hydrology and accretion and erosion, particularly in snowmelt-dominated systems. Annual hydrologic trends including the magnitude, frequency, timing, duration, and rate of change in discharge are important aspects of river flow regimes (N. LeRoy Poff et al., 1997) that facilitate erosion and deposition in channels and along floodplains (Wohl et al., 2015). Field observations and remotely sensed imagery have been used to quantify bank erosion and lateral accretion and to better understand planform change and river dynamics associated with changes in water and sediment supply (James E. Pizzuto, 1994; Micheli & Kirchner, 2002a, 2002b; S. S. Day et al., 2013b, 2013a; Lenhart et al., 2013; J. C. Rowland et al., 2016; Schook et al., 2017; Schwenk et al., 2017; Caponi et

al., 2019; Grams et al., 2020), but detailed analysis of flow regimes have not been correlated with these observations.

Both lateral and vertical accretion have been negatively correlated with relative elevation and horizontal distance from the channel (G. Day et al., 2008; Hupp et al., 2008; Metzger et al., 2020), and studies examining hydrology have focused on peak discharge magnitude. Lateral accretion and channel narrowing have been attributed to periods of decreased mean peak flow in the snowmelt-dominated Green River (Grams et al., 2020). Moderate values of maximum annual peak discharge in the snowmelt-dominated Powder River, MT, has been linked to net floodplain deposition, whereas larger flows resulted in net erosion (James E. Pizzuto, 1994). Larger peak discharges in snowmelt-dominated systems facilitate germination of cottonwoods and point bar accretion (Schook et al., 2017; Metzger et al., 2020; James E. Pizzuto, 1994).

Linkages between hydrology and successful establishment of riparian vegetation influence point bar stabilization and accretion. Increased flood duration and slower recession limbs can regulate successful establishment of riparian vegetation (Merritt & Wohl, 2002; Nilsson et al., 2010; Benjankar et al., 2014; Caponi et al., 2019). The duration between bankfull flow events has been referred to as the “window of opportunity” for riparian vegetation to germinate and has been shown to be highly correlated with point bar accretion (Balke et al., 2014). Timing is crucial for the successful germination and establishment of cottonwood seedlings during the recession limb of snowmelt-dominated annual peak flows in the western US (Friedman et al., 1996; Mahoney & Rood, 1998; Merritt & Wohl, 2002; Nilsson et al., 2010). Morphological effects of changes in riparian vegetation and point bar accretion have been documented with regard to damming and river flow regulation (Cooper et al., 1999; Merritt & Cooper, 2000; N. Leroy Poff et al., 2010) and changes in hydrology associated with climate (Wolf et al., 2007; Schook et al., 2017). These relationships between hydrochory (water

dispersal of seeds) and point bar stabilization highlight the potential importance of timing of peak discharge, flood duration, and the slope of the recession limb on sediment dynamics in snowmelt dominated systems.

Examination of floodplain erosion commonly focuses on physically-based models that incorporate geomechanics to described three primary classes of bank erosion. Cantilever failures, planar shear, and slip or rotational failures arising from river bank undercutting due to excess bank shear stress, and destabilization due to positive pore pressures during bank drainage (Thorne & Tovey, 1981; Simon et al., 2000; Langendoen & Simon, 2008; Langendoen & Alonso, 2008).

A common fluvial geomorphic approach to quantify bank erosion and channel migration is to estimate or measure near-bank velocities (Parker et al., 1982; J. E. Pizzuto & Meckelnburg, 1989). This approach has provided a basis for estimating excess bank shear stress acting on channel margins as a function of flow depth (Partheniades, 1965; Darby et al., 2007). Other studies have found correlations between bank erosion rates and the radius of curvature (Hooke, 1980; Begin, 1981; Nanson Gerald C. & Hickin Edward J., 1983; Hooke, 2007) but direct correlations between these variables is seldom significant. Correlations with curvature have shown to be stronger when considering a smoothed average along bends, a decay function with increasing distance downstream, or a quasi-linear lag downstream (Furbish, 1991; Güneralp & Rhoads, 2009; Sylvester et al., 2019). Because reach sinuosity captures aspects of curvature, it is likely to influence bank erosion and channel migration.

Because the hydrologic aspects of bank erosion and migration modeling efforts mentioned above focus primarily on channel morphology and flow depth, consideration of other aspects of the flow regime are needed. Bank erosion and channel widening have been linked with the duration and magnitude of peak discharge (Hooke, 1979) and annual peak discharge in snowmelt-dominated systems (James E. Pizzuto, 1994). Some

bank erosion models consider the duration of flow (Langendoen & Alonso, 2008; Langendoen & Simon, 2008). Positive pore pressure of saturated banks combined with the loss of supporting pressure when stage declines make slip and rotational bank failures likely (Rinaldi & Casagli, 1999). These bank failures triggered by positive pore pressure are common in flashy systems dominated by rainfall and maximum annual peaks that decline within a single day, but this phenomenon does not typically occur in snowmelt-dominated systems where recession limbs span days to weeks. Detailed examination of the rate of change in snowmelt-dominated flows have not been examined in detail, but likely influence river bank stability and erosion on seasonal scales (Wolman, 1959; Simon et al., 2002). Thus, additional hydrologic indices such as the rate of change offer the potential to provide a more robust understanding of the hydrologic drivers of bank erosion.

In the literature cited above, many studies either provide detailed analysis of bank erosion at very small spatial scales (ie…a single bend) or long-term estimates of river migration and/or floodplain deposition at broad spatial scales. The spatially focused studies allows for direct attribution of geomorphic change to site-specific flow conditions, but commonly lack a longer term analysis of hydrology needed to integrate these results over time. Similarly, erosion and deposition studies often occur independently limiting the ability to attribute the hydrological drivers and timing to sediment fluxes to and from the floodplain.

Quantifying the unique hydrological drivers for erosion and deposition independently may facilitate the prediction of changes in net exchanges between rivers and floodplains under changing hydrological conditions. This is of particular importance under future climate change poised to greatly alter snowmelt-dominated river flow regimes (Adam et al., 2009). Insights on erosion and depositional controls in temperate snowmelt systems have direct relevance to river systems in the western US where >50%

of total runoff and 70% of mountainous runoff is derived from snow. River hydrology that is dominated by similar snowmelt-driven peak flows associated with spring thaw controls river dynamics across the northern high-latitudes (Adam et al., 2009; McClelland et al., 2012).

The objective of this research was to identify detailed aspects of the hydrologic flow regime (e.g., peak magnitude, duration, timing of peak, slope of the recession limb) that most significantly influence bank erosion and floodplain accretion in a snowmelt dominated system, while also accounting for differences in channel morphology (e.g., sinuosity, channel slope, width). Thus, we quantify both the rates and patterns of bank erosion and floodplain deposition across a large range of spatial and temporal scales. We also calculated a sediment budget to verify our accounting of eroded and accreted floodplain sediment. In doing so, we validate a simplified approach to estimate hydrologic influence on channel migration using remotely sensed imagery and historic hydrologic data.

The research presented here is motivated by our efforts to quantify carbon storage and dynamics in a mountainous region along the floodplain of the East River near Crested Butte, Colorado, USA, in order to better inform the incorporation of floodplain dynamics in Earth System models to better quantify terrestrial carbon dynamics. Potential for changes in hydrology of snowmelt-dominated systems as a result of climate change (Middelkoop et al., 2001; Adam et al., 2009; Schneider et al., 2013) and resulting shifts in sediment dynamics are poised to alter terrestrial organic carbon dynamics in snowmelt-dominated floodplains, where carbon storage is substantial (Sutfin et al., 2016; Sutfin & Wohl, 2017; Lininger et al., 2018, 2019).

## 2 Study Area

We studied an 11-km long segment of the East River approximately 3.5 km down valley from Gothic, CO, (Figure 1) near Crested Butte. At the downstream end of the study segment, the East River drains approximately 134 $km^2$ and has an annual average precipitation of 64 cm (SNOTEL, 2017). The study segment lies directly downstream of steep, confined, mountainous tributaries that incise through sandstones, mudstones, shales, granodiorite and metamorphosed byproducts of the uplifted White Rock pluton in the Elk Mountains of Colorado (Gaskill et al., 1991). Within the floodplain reach, the East River is a gravel-cobble bed, sinuous alluvial river approximately 20-m wide on average and bounded by lateral Pinedale glacial moraines, landslide deposits, and outcrops of Mancos Shale along the bed and valley walls. Sedges, grasses, and willows dominate the vegetation along the floodplain with isolated trees, dominantly blue spruce, scattered along the reach, but rarely located along the river banks. Throughout the floodplain, extensive beaver activity results in dams, lodges and the introduction of large wood from the surrounding hillslopes. Floodplain fine overbank sediment is dominated by silt-size particles with varying proportions of sand, clay, and minimal gravel content (Malenda et al., 2019). Beneath fine sediment, the floodplain is composed of gravel and cobbles, and contains lenses of finer, sorted material. Erosion of underlying gravels and undercutting of fine overbank sediment commonly result in cantilever failure of grass-covered blocks along the East River 11-km long study segment (Figure 1D, S1).

The East River is a snowmelt-dominated, gravel bed river. The annual hydrograph is characterized by a gradual rising limb as temperatures warm and snow melts in the spring months of April and May. An annual peak flow commonly occurs in the latter half of May or early half of June after peak snowmelt, followed by a gradual recession limb that takes place over weeks (21 days on average) at which discharge returns to baseflow conditions sometime between September and November. Although there is a dearth of data on the sediment regime near the study site, existing studies

further downstream provide some insight into the East River study segment. The East River channel bed surface is characterized by a median grain size of 0.09 m at the USGS Almont gauging station near the confluence with the Gunnison River ~25 km downstream from the study site (Andrews, 1984). Bed mobility analysis along the Gunnison near Grand Junction, CO indicates that bedload transport occurs when discharge is nearly half the bankfull flow (Pitlick & Steeter, 1998).

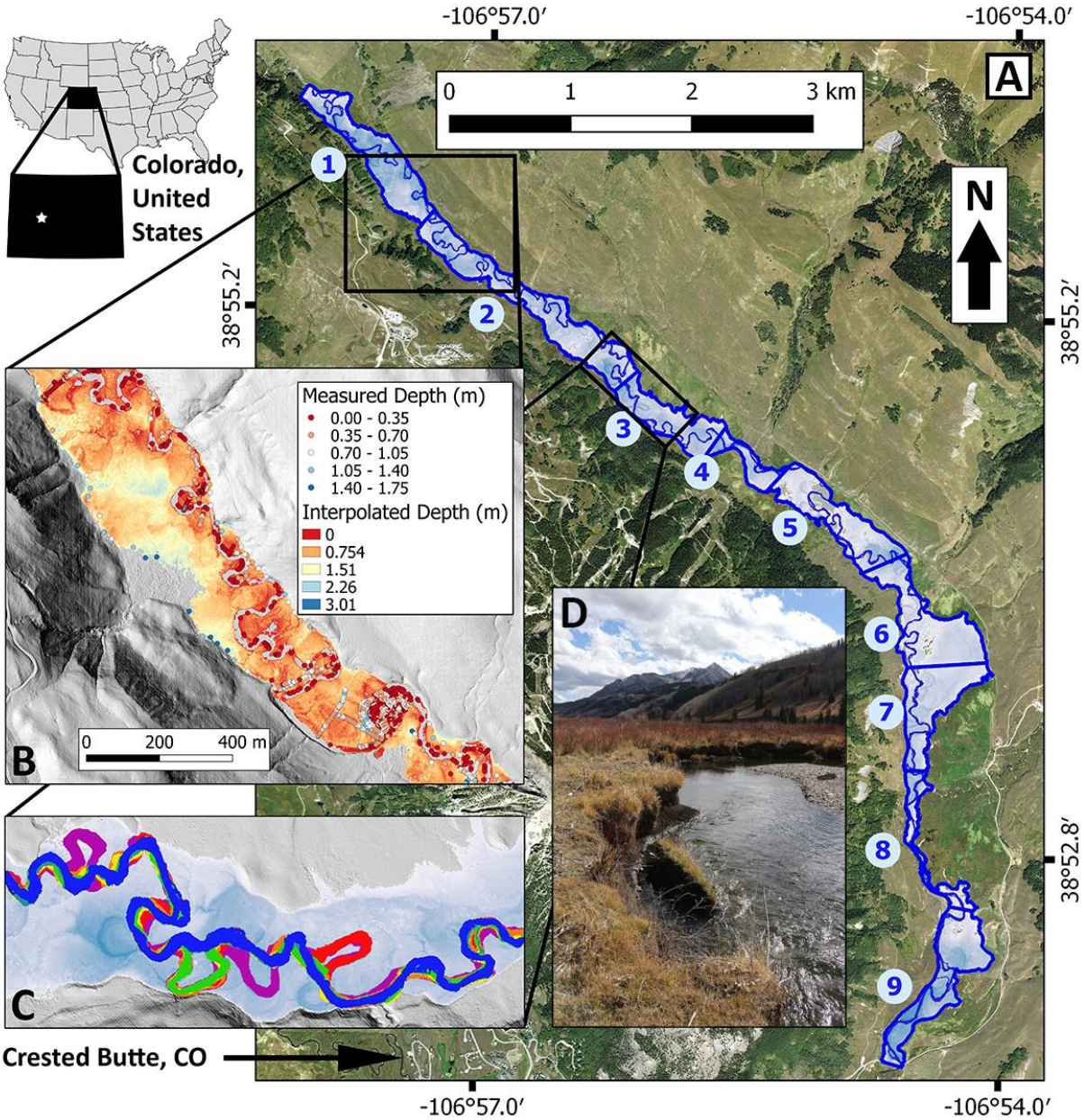


**Figure 1**. Map of study area on the East River near Crested Butte, Colorado, USA. The floodplain was delineated by "flooding" a 0.5-m resolution lidar digital elevation model

along the 11-km long study segment, which was divided into 9 study reaches (A) based on changes in valley slope. The depth of fine sediment was measured across the floodplain at 1847 points and interpolated across the upper 2 km, intensive study reach (B) consisting of reach 1 and approximately half of reach 2, ending at the downstream extent of the black box in (A). Masks of the river channel, depicted in various colors, were derived for all seven time periods (C), and used to determine lateral accretion and erosion, typically occurring as cantilever failures in the study area (D). Shades of blue beneath the channel masks in C indicate relative depth of water across the delineated floodplain, from which previous channel locations can be identified.

Limited land-use impacts have influenced the watershed upstream of the 11-km long study segment of the East River. From 1880 to 1890, a silver mine operated along Copper Creek upstream of Gothic, CO, the present location of the Rocky Mountain Biological Laboratory. The mining area is now designated as US Forest Service (USFS) national forest and wilderness area. Land use along the 11-km long study segment consists of small privately owned parcels and U.S. Forest Service (USFS) land, on which ranchers graze cattle for limited portions of the year (Theobald et al., 1996). Limited property access restricted our field investigations to the upper 2 km, intensive study reach (Figure 1A; Reach 1 and half of reach 2). Although flow diversions exist within the 11-km long study segment, they were present prior to beginning of the study period in 1955 and they primarily capture runoff from tributaries before they reach the East River.

## 3 Materials and Methods

Spatial analysis of aerial lidar, repeat aerial imagery, historical hydrologic flow analysis, surface water flow measurements, measurements of floodplain fine sediment depth, and multiple linear regression were used to estimate a sediment budget and examine linkages between hydrology and bank erosion, accretion, and channel migration rates over 60 years (Figure 2).

### *3.1 Terrain Analysis and Study Reach Delineation*

242 Aerial lidar was collected in August of 2015 for the entire East River watershed
243 (Wainwright & Williams, 2017) and was used for all topographic analysis.. Average bare-
244 ground point cloud density of lidar was 4.29 points/$m^2$ resulting in a total accuracy with
245 root mean squared error of 0.05 m at the 95% confidence level. A hydro-flattened, bare-
246 ground DEM with a horizontal resolution of 0.5 m was derived from the lidar point cloud
247 data. Based on local valley slope, we divided the ~11-km long floodplain segment into
248 nine study reaches. We calculated the valley slope using a best-fit line of elevation
249 points extracted from the 2015 DEM and spaced every 10 meters down the valley
250 center. We detrended the slope of the 9 sub-reaches using the raster calculator in QGIS
251 and recombined them to generate a floodplain DEM with zero down-valley slope and a
252 maximum total relief of 5.44 m. We artificially entrenched the flat lidar water surface by 2
253 meters and used the *r.fill.dir* Grass tool in QGIS to flood the detrended DEM at a depth
254 of six meters to delineate the approximate extent of the floodplain. We verified the
255 digitally delineated floodplain extent with field observations of distinct breaks in slope,
256 such as the base of lateral moraines, toes of alluvial fans, and abutments to incised
257 bedrock outcrops.

258 *3.2 Channel Position and Movement using Aerial Imagery*

259 We used aerial images from six dates (i.e., 1955, 1973, 1983, 1990, 2001, 2012)
260 obtained from the US Geological Survey, US Department of Agriculture, and the US
261 Forest Service, and satellite imagery from 2015 to quantify morphological change over
262 time (Figure S2). All imagery was resampled to 1-m resolution to allow direct comparison
263 between images. We georeferenced the 2015 imagery using the 2015 lidar DEM dataset
264 as a reference using >6 control points including the corners of buildings, intersections of
265 roads and fences, and the base of mature trees. All other images were georeferenced (if
266 not already done so by the source agency) through comparison with similar point types
267 in the 2015 georeferenced image.

To analyze channel characteristics and compare changes over time, we generated binary channel masks for each set of aerial imagery (Rowland & Stauffer, 2020). For color imagery between 1973 and 2015, we generated masks of bankfull river extent using red-green-blue (RGB) color bands and the normalized difference water index (NDWI) to classify the channel water surface in each image (Figure 1C; McFeeters, 1996) using the object-oriented classification software, eCognition. To control for variations in water levels between images, regions of tan and grey gravel and sand bars devoid of vegetation and exposed, un-vegetated bank faces were included in the channel mask as an estimate of bankfull extent (Gurnell, 1997; Richard et al., 2005; Mount & Louis, 2005; Fisher et al., 2013; J. C. Rowland et al., 2016; Donovan et al., 2019). The black and white 1955 USDA photos required manual delineation of the channel mask.

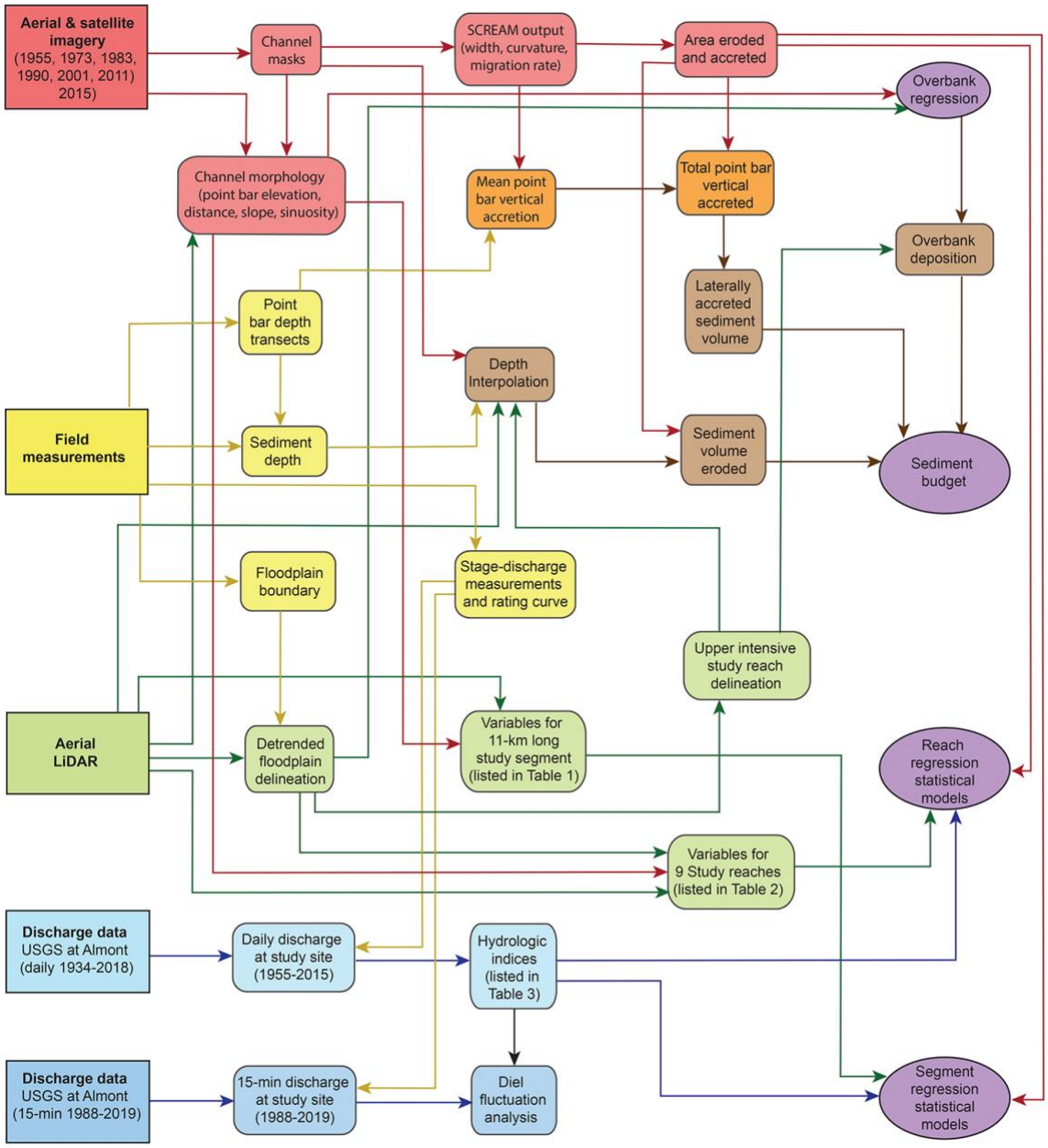


**Figure 2** Data sets used and generated for resulting analyses

Metrics calculated to quantify the channel and floodplain attributes for the nine valley reaches and entire 11-km long study segment included: valley, floodplain, and channel areas; valley and channel lengths; elevation change along the reach; valley and channel slopes; sinuosity; average channel width; and valley confinement. The channel area relative to the area of delineated valley floor defined valley confinement as a proxy

for potential of the floodplain to accommodate channel migration, dissipate energy during overbank flow, and facilitate overbank deposition. Channel sinuosity measures the channel length divided by the straight down-valley length. Channel slope was calculated as the valley slope divided by channel sinuosity.

Linear erosion, and accretion rates were determined for each bank pixel using the Spatially Continuous Riverbank Erosion and Accretion Measurements algorithm (SCREAM; Rowland et al., 2016, Rowland and Stauffer, 2020b). Linear rates represent the distance that a river bank face moves in a given time interval by measuring the Euclidean distance between a bank pixel in one river mask and the closest bank pixel at the subsequent river mask. Eroded and accreted floodplain areas derived from SCREAM were divided by the number of years within that time period and the channel length to estimate linear rates of erosion and accretion. Three sources of error are associated with our measurements of linear change: image registration, image classification and the accuracy of SCREAM output (Rowland et al., 2016). Average estimated registration error for the 1-m imagery from 1973 to 2015 was 0.58 m. Poor image quality of the 1955 photographs prevented direct estimates of error using this method, so we have assigned a registration error equal to two times the highest error (1.2 m) in areas for the period between 1955-1973. Errors associated with area-based erosion and accretion measurements as a result of image mis-registration for each time period were assigned as percentage of change in areas following the methodology detailed in Rowland et al. (2016). Total measurement errors were estimated by combining registration, classification, and methodological errors in quadrature (Rowland et al. 2016)) (Table S1).

*3.3 Vertical Accretion Rates*

We estimated long-term point bar vertical accretion rates using a combination of field-based measurements of fine-grained deposit thickness and changes in channel

position from aerial imagery between 1973 and 2015. Images from 1955 were excluded from this analysis because of the uncertainty associated with the poor-quality images. In 2016, along the upper 2 km, intensive study reach (Figure 1A, reach 1 and half of reach 2), we measured thickness of fine-grained deposits at 324 locations on 21 transects by inserting a soil probe into the floodplain surface until refusal at bedrock or gravel-size material (>2mm) (Sutfin & Rowland, 2019). Mean migration rate was estimated from SCREAM output along bends (Figure S3) and the distance between each transect point and the channel was converted into duration since channel occupation by dividing by the bend averaged migration rate. We used the total depth in locations previously occupied by the channel to represent an average point bar deposition rate over each time period examined. The measured depth of fine sediment ($d_i$) was then divided by the duration since occupation by the river channel ($t_i$, when fine sediment depth would have been equal to zero) to estimate a mean vertical accretion rate ($a_i$; Equation 1).

$$\overline{a_i} = \frac{d_i}{t_i} \quad (1)$$

Potential predictors of overbank vertical accretion rates, across the upper 2 km, intensive study reach were assessed through stepwise multiple linear regression. Variables examined for this analysis were similar to those described above, with the following additions. Distance from the channel was measured in the field. Relative elevation from the bankfull stage at the transect was extracted from the lidar at the top of point bars where bar sand/gravel transitioned into vegetation cover. Along each transect, channel width, valley width, and the ratio between the two (valley confinement) were measured from the imagery in GIS. Localized valley slope, channel slope, and sinuosity were measured using GIS extending approximately 50 m upstream to 50 m downstream of the transect. Mean values of radius of curvature, lateral accretion rate, and erosion rate were calculated along each meander bend. Measurements were denoted as either

being on the inside or outside of a bend. The angle of each transect was used as a proxy for the angle of each river bend relative to the down valley direction from 0-90º.

*3.4 Estimating floodplain sediment volumes*

We estimate volumes of fine grained (less ~ 2mm in grain diameter) sediments deposited on top of the gravel-rich channel and point bar deposits. In addition to the soil probe measurements collected on point bar transects (Section 3.3), 1,587 measurements were made along the upper 2 km intensive study reach (Figure 1A, Reaches 1 and 2; Sutfin & Rowland, 2019). We subtracted these depth measurements from the DEM elevations using the *raster calculator* in QGIS to calculate an absolute elevation of underlying gravel/bedrock. We then generated a triangular irregular network (TIN) of the gravel-bedrock surface elevation using the *interpolate* tool in QGIS. By subtracting elevations of this interpolated surface from the ground surface elevations, we created a spatially continuous isopach map of fine-grained floodplain sediment. The interpolated depth of fine sediment was zero in areas occupied by the 2015 channel. To correct for this we used the *close gap* Saga tool in QGIS (threshold = 0.1). The thickness of fine-sediment thickness during 2015 was interpolated across the channel using a 3 m buffer that extended beyond the locally thin deposits covering active point bars. This estimated sediment depth available for erosion in previous years. We calculated eroded volumes by multiplying the areas of eroded regions derived from the aerial imagery for each time interval by the interpolated isopach map of fine sediment within those mapped areas.

Using the estimated vertical accretion rates from our soil probe transects we estimated an average deposition rate for laterally accreted regions along the channel and developed a multiple linear regression model to estimate overbank deposition on the stable floodplain surface. For the laterally accreted areas, we used the average migration rates at bends described above in section 3.3. This approach determined the

364 portion of contemporary floodplain that would have been formed by lateral accretion for
365 the entire period between 1973-2015. A reach-based average migration rate and
366 resulting mean migration distance along the probe transects were used to estimate an
367 average vertical accretion rate from all points within the mean migration distance during
368 the 42 years (Table S2). This average rate was multiplied by the mapped accretion
369 areas from the aerial photos and SCREAM output to provide a volume of laterally
370 accreted sediments.

371 Overbank deposition rates beyond 10 m were calculated for each cell using a
372 multiple linear regression model including only the two strongest predictor variables,
373 distance from the channel and relative elevation from the channel (Figure S4). The
374 *proximity grid* Saga tool in QGIS was used to create a grid based on distance from the
375 channel for images from the six years. Floodplain elevation relative to the channel was
376 calculated by subtracting the minimum elevation from the detrended 2015 DEM
377 floodplain surface (derivation described above in section 3.1). This assigned a relative
378 elevation to every raster pixel. The river channel buffered by three meters on both sides
379 was subtracted from the relative elevation grid and the *close gap* tool in QGIS was used
380 to interpolate elevations across the channel.

381 The distance-from-channel raster and the detrended-valley DEM were used as
382 input to the vertical accretion rate regression model equation in the raster calculator to
383 generate raster grids of estimated overbank deposition rates for all six time periods.
384 Overbank sediment deposition estimates of volume were made by multiplying calculated
385 rates by the number of years in the respective time interval, summing all pixel values for
386 each period, and multiply that value by the area of each pixel (0.25 $m^2$). Vertical
387 accretion within abandoned channels was estimated using the vertical accretion rate of
388 0.033 m $y^{-1}$ within the first 10 m from the channel for periods following cutoff occurrence.
389 Aggradation of previously abandoned channels was based on the relative vertical and

horizontal distance from the active bankfull channel at distances exceeding 10 m. Rates of volume of sediment accreted and eroded during each time period were estimated by dividing the total volume of sediment by the number of years in each time period.

*3.5 Streamflow Data and Hydrologic Analysis*

Streamflow was measured 22 times near the Crested Butte city water pump house in the upper 2 km, intensive study reach, from October, 1$^{st}$, 2014, to September, 30$^{th}$, 2017, and a stage-discharge rating curve was created against stage data recorded every 15 minutes ($r^2$ = 0.99) (Carroll & Williams, 2019). To extend the flow record prior to 2014, we regressed measured discharge at the 2-km intensive study reach against data from the US Geological Survey stream gage on the East River at Almont (gage # 09112500) 25 km downstream ($r^2$ = 0.97; Figure 4A). Using this regression, we generated a synthetic hydrograph for the study site from 1934-2018 using the Almont streamflow data (Table S3). A comparison of the synthetic hydrograph and flows measured between 2014 and 2018 showed a strong agreement with a Nash-Sutcliffe Efficiency coefficient (NSE) of 0.97 (Figure 4B). Flow frequency analysis was conducted on the entire synthetic hydrograph to determine annual statistics for the continuous 82 years. Analysis of possible hydrological drivers for erosion and deposition examined the synthetic hydrograph from 1955 to 2015 to correspond with the aerial imagery analysis.

We used R software (R Core Team, 2017) to extract synthetic hydrograph characteristic between 1955 and 2015. An average minimum flow value of 0.49 $m^3$ $s^{-1}$ during the low-flow months of October, November, December, January, February, and March were used as a reference baseflow condition. Bankfull flow was estimated as 8 $m^3$ s-1 based on field observations and hydrologic analysis indicates an approximate recurrence interval of 1.2 years. The mean value for the day of the year on which peak flow occurred, the last day exceeding bankfull flow conditions, and the last day exceeding baseflow conditions were calculated for each time period. The maximum and

mean values within each time period were calculated for annual hydrograph peak magnitude, peak timing, annual volume of discharge, the annual volume of water above bankfull flow, duration between the first and last day of flow exceeding baseflow, the number of days on which baseflow occurred, the annual volume of discharge exceeding bankfull, duration between the first and last day of flow exceeding bankfull flow, the number of days on which bankfull flow occurred, and the cumulative number of days since the last bankfull flow, the total recession slope from the annual maximum peak to baseflow (herein referred to as the total recession slope), the bankfull recession slope from bankfull stage to baseflow (herein referred to as the bankfull recession slope), and the number of peaks above bankfull flow. Recession slopes were estimated as the positive slope of the line between peak of bankfull discharge and the first occurrence of baseflow conditions.

An additional analysis was conducted to examine diel fluctuations in discharge associated with the slope of the recession limb of each annual hydrograph. A regression analysis of 15-minute streamflow data from the same USGS gauge and measured flow at the study site from 2015-2019 yielded an $r^2 = 0.94$. This regression was used to extend the study site discharge data to span the duration of the 15-minute data from 1988-2018. Hourly data were extracted from this 15-minute discharge data and the maximum and minimum daily values were determined for years with peak annual flow exceeding 6 $m^3s^{-1}$. On days with maximum flows below 10 $m^3s^{-1}$ and minimum flow above 5 $m^3s^{-1}$ the number and magnitude of diel fluctuations greater than 2 $m^3s^{-1}$ were summed. Correlations were examined between the maximum recession slope and the number, the summed magnitude, and the average magnitude of diel fluctuations to occur within the defined recession window.

*3.6 Statistical Analyses*

The number of potential variables for all multivariate regression models used to identify significant predictors was reduced to minimize collinearity of predictor variables prior to multiple linear regression. Starting with the most strongly correlated variable and working sequentially through variables with decreasing correlation values, variables were eliminated as potential predictors for the regression model if they were moderately cross correlated ($r > 0.7$) with another more strongly correlated variable (Dormann et al., 2013) already selected as a predictor. Stepwise multiple linear regression was conducted using the *stats* package *lm* function in R statistical software to examine possible predictor variables and determine the best regression model for: (1) the area of accreted and (2) the area of eroded floodplain along nine study reaches, and (3) vertical floodplain deposition rate estimated from measurements of floodplain fine sediment depth along the upper 2 km, intensive study reach over the 6 time periods. Multiple linear regression assumptions of normality and homoscedasticity of model residuals were met with power transformations and verified using the Shapiro-Wilk normality test (*shapiro.test* function) and the non-constant error variance test in R (*ncv.test* function), for which details are provided in supporting material. Variables were included in stepwise multiple linear regression to identify the best regression model based on minimizing the Akaike Information Criteria (AIC).

In addition to the stepwise linear regression for all nine study reaches in the six time periods, we examined univariate correlations between hydrologic variables and both erosion and accretion during the six time periods along the entire 11-km study segment.

## 4. Results

### *4.1 Channel and floodplain metrics*

The floodplain delineation of the entire 11-km long study segment resulted in a valley bottom area of 2.65 $km^2$ with a total valley length of 10.62 km and a total valley slope of 0.64%. Despite the occurrence of 21 channel chute cutoffs in the 60-year time period, channel slope and the sinuosity for the entire river segment remained relatively constant during the six periods examined. Channel slope along the entire 11-km long study segment varied from 0.34% to 0.36% over the 60-year time period. Sinuosity fluctuated about a mean value of 1.81 $\pm$ 0.04 m/m (SD) with a minimum and maximum of 1.77 to 1.89 (Table 1).

**Table 1**. Morphological characteristics of the entire 11 km long study segment of the East River derived from remotely sensed imagery and lidar for each time period. Channel width was calculated as a mean of channel width pixel values from SCREAM and standard deviations of those averages are provided following each mean.

| Year | Floodplain area ($km^2$) | Channel Area ($km^2$) | Channel Length (km) | Sinuosity (m/m) | Channel slope (%) | Confinement ($m^2/m^2$) | Mean channel width (m) |
|---|---|---|---|---|---|---|---|
| 1955 | 2193.6 | 459.0 | 20.08 | 1.89 | 0.339 | 0.17 | 25 ± 2 |
| 1973 | 2254.0 | 398.7 | 19.29 | 1.82 | 0.353 | 0.15 | 20 ± 2 |
| 1983 | 2222.3 | 430.3 | 18.80 | 1.77 | 0.362 | 0.16 | 23 ± 3 |
| 1990 | 2295.4 | 357.3 | 18.90 | 1.78 | 0.361 | 0.13 | 19 ± 3 |
| 2001 | 2275.4 | 377.3 | 19.39 | 1.83 | 0.352 | 0.14 | 21 ± 3 |
| 2011 | 2296.2 | 356.5 | 18.81 | 1.77 | 0.362 | 0.13 | 19 ± 1 |
| 2015 | 2312.2 | 340.4 | 18.98 | 1.79 | 0.359 | 0.13 | 17 ± 1 |

**Table 2**. Morphological characteristics of nine study reaches derived from remotely sensed imagery and lidar. Values are averaged from the seven images spanning 60 years and standard deviations of those averages are provided following each mean.

| Reach | Valley area ($m^2$) | Valley Length (m) | Valley slope (%) | Floodplain area ($m^2$) | Channel Area (m2) | Channel Length (m) | Sinuosity (m/m) | Channel slope (%) | Confinement ($m^2/m^2$) | Channel width (m) |
|---|---|---|---|---|---|---|---|---|---|---|
| 1 | 344236 | 1471 | 0.94 | 294462 | 49774 ± 6292 | 2860 ± 130 | 1.94 ± 0.09 | 0.48 ± 0.02 | 0.14 ± 0.02 | 18 ± 3 |
| 2 | 489119 | 2126 | 0.74 | 405784 | 83334 ± 6234 | 4735 ± 143 | 2.23 ± 0.07 | 0.33 ± 0.01 | 0.17 ± 0.01 | 18 ± 2 |
| 3 | 232658 | 910 | 0.55 | 199873 | 32785 ± 6046 | 1740 ± 99 | 1.91 ± 0.11 | 0.29 ± 0.02 | 0.14 ± 0.03 | 19 ± 3 |
| 4 | 93445 | 595 | 0.86 | 76134 | 17311 ± 1495 | 903 ± 60 | 1.52 ± 0.10 | 0.57 ± 0.04 | 0.19 ± 0.02 | 20 ± 2 |
| 5 | 330488 | 1142 | 0.68 | 283494 | 46994 ± 5334 | 2419 ± 170 | 2.12 ± 0.15 | 0.32 ± 0.02 | 0.14 ± 0.02 | 20 ± 2 |
| 6 | 378666 | 924 | 0.56 | 344169 | 34497 ±4194 | 1448 ± 248 | 1.57 ± 0.27 | 0.37 ± 0.06 | 0.09 ± 0.01 | 22 ± 3 |
| 7 | 302210 | 855 | 0.33 | 271371 | 30839 ± 6166 | 1490 ± 116 | 1.74 ± 0.14 | 0.19 ± 0.02 | 0.10 ± 0.02 | 21 ± 3 |
| 8 | 126101 | 1175 | 0.54 | 89108 | 36992 ± 2469 | 1583 ± 26 | 1.35 ± 0.02 | 0.40 ± 0.01 | 0.29 ± 0.02 | 23 ± 3 |
| 9 | 355743 | 1420 | 0.46 | 299779 | 55965 ± 8114 | 2001 ± 53 | 1.41 ± 0.04 | 0.33 ± 0.01 | 0.16 ± 0.02 | 23 ± 4 |

Valley slope ranged from 0.33% to 0.94% along each of the 9 delineated study reaches with a mean of 0.36 ± 0.19% (SD; Table 2). Mean valley confinement for the time period was 0.16 ± 0.02 $m^2/m^2$ (mean ± SD). Study reach 8 is the most confined reach ($C_v$ = 0.29 ± 0.02) and is located toward the downstream end of the 11-km long study segment where the tributary alluvial fan from Brush Creek constricts the East River valley. Reach sinuosity (P) averaged over the time period is also lowest in study reach 8 at 1.35 ± 0.02 m/m (Figure 3). The highest reach mean sinuosity (P = 2.23 ± 0.07) occurred in reach 2, which is moderately confined ($C_v$ = 0.17 ± 0.01) (Table 2).

Averaged over all time periods, channel width generally increased from upstream reaches to downstream reaches (Table 2), but fluctuated through time across the entire study segment. Although the channel mean width fluctuated with intervals of widening followed by narrowing, there was a net overall decrease over the 60-year time period. The average channel width for the entire 11-km long study segment decreased from a high of 25 ± 2 m in 1955 to a minimum of 17 ± 1 m in 2015. The greatest width reduction (~5 m) occurred between 1955 and 1973, but a substantial decreased of >4 m also occurred during two time periods between 2001 and 2015.

*4.2 Channel Migration and Floodplain Area*

The net balance between total area of eroded and accreted floodplain by the East River varied over the six time periods, with estimated accretion greater than erosion in four out of six time periods (Table 3). Over the entire 60-year period accretion exceeded erosion by 120,036 **±** 43,973 $m^2$, equal to 5.3% of the total area of the valley bottom. This accretion total includes the area of 21 abandoned channels arising from meander bend cutoffs. The highest rate of change in floodplain sediment balance occurred from 1983-1990 with a mean accretion rate outpacing erosion by a factor of four (Table 3; Figure 3). There was an observed decrease in channel width during this period, followed by a period dominated by erosion and channel widening. The

period between 1973 and 1983 was dominated by the largest erosion rates observed in this study, and was accompanied by an observed increase in channel width (Table 1, 3; Figure 3A).

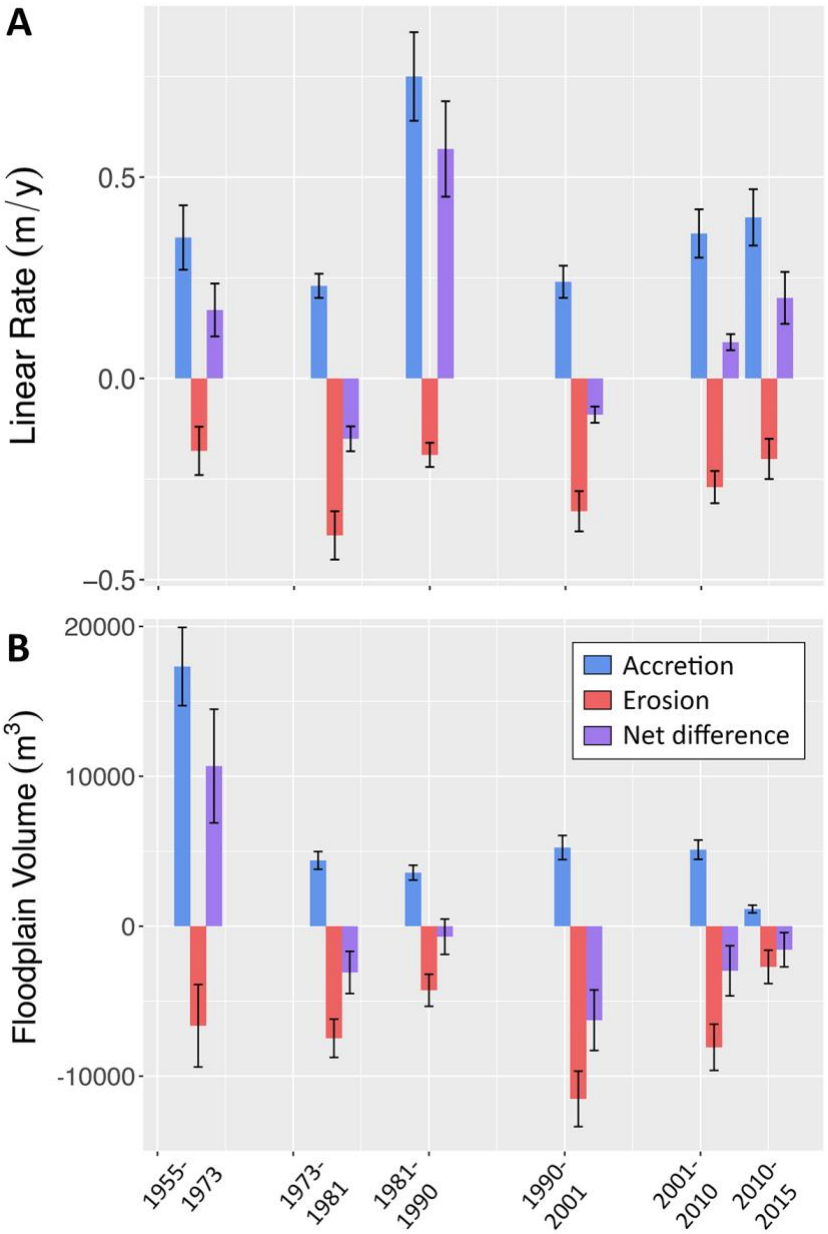


**Figure 3** Bar plots of estimated accretion, erosion, and net difference (accretion minus erosion) in linear rates along the entire 11-km long study segment (A) and volume of floodplain fine sediment along the upper 2 km, intensive study reach (B) during each time period examined over the 60 year study period.

520 **Table 3.** Area accreted and eroded across the entire 11-km long study segment and hydrologic

521 flow indices on the East River during the six time periods of the study.

| | 1955-1973 | 1973-1983 | 1983-1990 | 1990-2001 | 2001-2011 | 2011-2015 | Mean | Total |
|---|---|---|---|---|---|---|---|---|
| **Duration (years)** | 18 ± 0.3 | 10 ± 0.3 | 7 ± 0.3 | 11 ± 0.3 | 10 ± 0.3 | 4 ± 0.3 | 10 ± 0.3 | 60 ± 0.8 |
| **Accretion ($m^2$)** | 125529 ± 27774 | 45276 ± 6339 | 99194 ± 13887 | 50226 ± 8036 | 70686 ± 9189 | 30156 ± 7539 | 70178 ± 12127 | 421067 ± 34789 |
| **Erosion ($m^2$)** | -64915 ± 25388 | -74670 ± 12694 | -24569 ± 6142 | -69550 ± 11128 | -52358 ± 9948 | -14969 ± 6137 | -50172 ± 11906 | -301031 ± 33224 |
| **Net Change ($m^2$)** | 60614 ± 37629 | -29394 ± 14188 | 74625 ± 15185 | -19324 ± 13726 | 18328 ± 13543 | 15187 ± 9721 | 20006 ± 17332 | 120036 ± 48106 |
| **Accretion Rate ($m^2y^{-1}$)** | 6974 ± 1548 | 4528 ± 652 | 14171 ± 2095 | 4566 ± 744 | 7069 ± 949 | 7539 ± 1987 | 7474 ± 1329 | 44846 ± 3551 |
| **Erosion Rate ($m^2y^{-1}$)** | -3606 ± 1412 | -7467 ± 1294 | -3510 ± 893 | -6323 ± 1030 | -5236 ± 1010 | -3742 ± 1566 | -4981 ± 1201 | -29884 ± 2999 |
| **Mean linear Accretion Rate ($m\ y^{-1}$)** | 0.347 ± 0.077 | 0.235 ± 0.034 | 0.754 ± 0.111 | 0.242 ± 0.039 | 0.365 ± 0.049 | 0.401 ± 0.106 | 0.390 ± 0.069 | 2.343 ± 0.186 |
| **Mean Linear Erosion Rate ($m\ y^{-1}$)** | -0.180 ± 0.070 | -0.387 ± 0.067 | -0.187 ± 0.048 | -0.334 ± 0.054 | -0.270 ± 0.052 | -0.199 ± 0.083 | -0.259 ± 0.062 | -1.557 ± 0.156 |
| Mean Day of Peak Flow | 152.7 | 162 | 156.3 | 151.5 | 147 | 155.3 | 154.13 ± 5.06 | |
| Mean Peak Flow ($m^3s^{-1}$) | 11.84 | 11.6 | 12.9 | 12.35 | 11.31 | 10.15 | 11.69 ± 0.94 | |
| Max Peak Flow ($m^3s^{-1}$) | 22.56 | 18.32 | 21.86 | 23.74 | 16.02 | 15.49 | 19.67 ± 3.53 | |
| Mean Bankfull Duration (days) | 31.3 | 38.1 | 41 | 36.1 | 29.3 | 25.5 | 33.55 ± 5.84 | |
| Max Bankfull Duration (days) | 61 | 48 | 64 | 63 | 47 | 31 | 52.33 ± 12.86 | |
| Mean Days Above Bankfull Flow | 20.3 | 24 | 22.6 | 23.8 | 18.5 | 12.8 | 20.33 ± 4.26 | |
| Max Days Above Bankfull Flow | 59 | 46 | 62 | 56 | 47 | 30 | 50.00 ± 11.71 | |
| Mean Duration Above Baseflow (days) | 215.5 | 218 | 255.1 | 230.9 | 263 | 278.5 | 243.50 ± 25.82 | |
| Max Duration Above Baseflow (days) | 362 | 331 | 364 | 305 | 364 | 349 | 345.83 ± 23.74 | |
| Mean Days Above Baseflow | 232.1 | 217.8 | 266.7 | 243.9 | 259.8 | 245.5 | 244.30 ± 17.86 | |
| Max Days Above Baseflow | 281 | 261 | 362 | 275 | 316 | 272 | 294.50 ± 37.97 | |
| Mean Days Since Bankfull Flow | 267 | 327.1 | 349.6 | 261.3 | 345.3 | 455.3 | 334.27 ± 70.58 | |
| Max Days Since Bankfull Flow | 925 | 904 | 935 | 579 | 944 | 901 | 864.67 ± 140.96 | |
| Mean Day Baseflow Ends | 280.2 | 288.6 | 304 | 305.3 | 291 | 321.3 | 298.40 ± 14.73 | |
| Mean Day Bankfull Flow Ends | 173.3 | 181.9 | 176.8 | 172.7 | 170.3 | 173 | 174.67 ± 4.11 | |
| Mean No. Peaks Above Bankfull | 1.9 | 1.9 | 2 | 1.8 | 1.4 | 0.5 | 1.52 ± 0.61 | |
| Maximum No. Peaks Above Bankfull | 3 | 4 | 5 | 4 | 3 | 1 | 3.33 ± 1.37 | |
| Mean Total Recession Slope ($m^3\ s^{-1}\ day^{-1}$) | 0.094 | 0.087 | 0.083 | 0.077 | 0.079 | 0.056 | 0.08 ± 0.01 | |
| Max Total Recession Slope ($m^3\ s^{-1}\ day^{-1}$) | 0.149 | 0.142 | 0.097 | 0.13 | 0.124 | 0.085 | 0.12 ± 0.03 | |
| Mean Bankfull Recession Slope ($m^3\ s^{-1}\ day^{-1}$) | 0.076 | 0.064 | 0.059 | 0.058 | 0.066 | 0.047 | 0.06 ± 0.01 | |
| Max Bankfull Recession Slope ($m^3\ s^{-1}\ day^{-1}$) | 0.12 | 0.086 | 0.082 | 0.075 | 0.091 | 0.05 | 0.08 ± 0.02 | |
| Mean Total Annual Volume ($km^3$) | 0.060 | 0.059 | 0.067 | 0.065 | 0.057 | 0.051 | 0.060 ± 0.006 | |
| Max Total Annual Volume ($km^3$) | 0.109 | 0.081 | 0.103 | 0.110 | 0.087 | 0.077 | 0.094 ± 0.015 | |
| Mean Bankfull Volume ($km^3$) | 0.027 | 0.034 | 0.037 | 0.033 | 0.027 | 0.024 | 0.031 ± 0.005 | |
| Max Bankfull Volume ($km^3$) | 0.074 | 0.047 | 0.072 | 0.073 | 0.050 | 0.031 | 0.058 ± 0.018 | |

522

*4.3 Floodplain Vertical Accretion*

Measured total depths of floodplain fine sediment above gravel and bedrock across the floodplain ranged from 0 to 1.41 m with a mean value of 0.41 ± 0.25 m (Table S2). A reach-based average migration rate of 0.24±0.05 m $y^{-1}$ resulted in a mean migration distance of ~10.0±2.1 m along the probe transects for the entire period between 1973-2015 (Table S2). Error presented in the values above were propagated from the mean standard deviation of the estimated mean migration rates derived from the SCREAM analysis. Using our estimated vertical accretion rates at each point, we estimated an average vertical accretion rate of 0.033±0.003 m $y^{-1}$ among all points within the closest 10 m from the channel. The best performing multiple linear regression model explains ~60% of the variability in vertical accretion rates ($r^2$=0.60, p<0.001) using distance from the channel, relative elevation from the channel, valley confinement, local channel slope (all with p<0.001), and whether the survey point was on the inside of a bend (p=0.023; Table S4). A cell-by-cell multiple linear regression model of estimates of vertical accretion rates ($r_{va}$) across the floodplain (Figure S3) for each time period was developed based on distance from the channel (p< 0.001) and relative elevation from the channel (p<0.001). This model explained ~54% of the variability in long-term vertical accretion rates over the 42-year time period between 1973 and 2015 ($r^2$=0.54, p<0.001) such that more deposition occurred closer to the channel and at lower elevations across the floodplain (Figure S3).

*4.4 Eroded and Accreted Sediment Volumes*

Estimated volumes of eroded and accreted sediment from the upper 2 km, intensive study reach were used to examine changes in volumes of floodplain sediment over the six time periods. Sediment input to and output from the floodplain during the six time periods ranged from 1145 ±258 to 17,324 ±2610 $m^3$ and 2713 ±113 to 11519 ±1851 $m^3$, respectively (Table 4). The difference between accreted and eroded volumes represent the net sediment change,

548 which ranged from -6273 ±2018 (where negative values indicate net erosion) to 10,683 ±3792
549 $m^3$ of sediment (Figure 3B, Table 4).
550 Estimated eroded volume exceeded accreted volume in all but one (i.e., 1955-1973) of
551 the six periods resulting in a net loss of sediment over the total 60-year time period (Figure 3B).
552 Although the resulting estimated sediment balance after 60 years was a net loss of 3919±5091
553 $m^3$ across the floodplain, this net difference falls within the error of the estimate and suggest
554 closure of the sediment budget.

**Table 4**. Floodplain area and sediment volume eroded, accreted, and the net change between accretion and erosion along the upper 2 km, intensive study reach.

| | 1955 - 1973 | 1973 - 1983 | 1983 - 1990 | 1990 - 2001 | 2001 - 2011 | 2011 - 2015 | Total |
|---|---|---|---|---|---|---|---|
| Duration (y) | 18 ± 0.3 | 10 ± 0.3 | 7 ± 0.3 | 11 ± 0.3 | 10 ± 0.3 | 4 ± 0.3 | |
| Area eroded ($m^2$)[a] | 12228 ± 5060 | 12428 ± 2113 | 7341 ± 1835 | 16774 ± 2684 | 13317 ± 2530 | 3752 ± 1538 | |
| Mean Depth of Eroded bank material (m) | 0.54 ± 0.01 | 0.60 ± 0.01 | 0.58 ± 0.01 | 0.69 ± 0.01 | 0.61 ± 0.01 | 0.72 ± 0.01 | |
| **Volume Eroded ($m^3$)[b]** | **-6640 ± 2751** | **-7476 ± 1277** | **-4272 ± 1071** | **-11519 ± 1851** | **-8080 ± 1541** | **-2713 ± 1113** | **-40700 ± 4169** |
| Mean erosion rate ($m^3$/y) | -369 ± 153 | -748 ± 130 | -610 ± 155 | -1047 ± 171 | -808 ± 156 | -678 ± 283 | |
| Mean bank area erosion rate ($m^2$/y)[c] | -0.02 ± 0.01 | -0.04 ± 0.01 | -0.03 ± 0.01 | -0.06 ± 0.01 | -0.04 ± 0.01 | -0.04 ± 0.02 | |
| Point bar area of accretion from ($m^2$)[d] | 28392 ± 4356 | 12391 ± 1735 | 14534 ± 2035 | 13612 ± 2178 | 14493 ± 1884 | 7403 ± 1851 | |
| Mean vertical accretion within eroded areas (m)[e] | 0.59 ± 0.01 | 0.33 ± 0.01 | 0.23 ± 0.01 | 0.36 ± 0.01 | 0.33 ± 0.01 | 0.13 ± 0.01 | |
| Estimated accretion along point bars ($m^3$)[f] | 16865 ± 2608 | 4089 ± 587 | 3357 ± 493 | 4941 ± 803 | 4783 ± 640 | 977 ± 255 | |
| Overbank deposition ($m^3$)[g] | 459 ± 92 | 302 ± 61 | 213 ± 44 | 305 ± 62 | 322 ± 66 | 168 ± 36 | |
| **Total volume accreted ($m^3$)[h]** | **17324 ± 2610** | **4391 ± 590** | **3570 ± 495** | **5246 ± 806** | **5105 ± 643** | **1145 ± 258** | **36780 ± 2921** |
| Mean accretion rate ($m^3$/y) | 962.43 ± 145.87 | 439.11 ± 60.462 | 509.97 ± 73.961 | 476.9 ± 74.406 | 510.54 ± 66.126 | 286.16 ± 67.924 | |
| **Net volume ($m^3$)** | **10684 ± 3792** | **-3085 ± 1407** | **-702 ± 1179** | **-6273 ± 2018** | **-2975 ± 1670** | **-1568 ± 1142** | **-3920 ± 5091** |

[a] Area eroded from banks estimated by SCREAM (Rowland et al., 2016)
[b] Volume calculated directly in GIS
[c] Mean vertical area of bank eroded estimated as the mean erosion rate divided by the total channel length
[d] Area of point bar accretion estimated by SCREAM
[e] Vertical accretion estimated as the product of the duration of each time period and accretion rates derived from measured probe transect of fine floodplain sediment depths described in section 3.3
[f] Volume of accretion estimated as the product of accreted areas identified by SCREAM and mean vertical accretion rates
[g] Estimates of overbank deposition derived from the regression model described in section 3.4 in which vertical accretion rates of each DEM cell were summed and the total was multiplied by the number of years in each time period.
[h] The sum of accreted volumes from point bars and overbank deposition

*4.5 Hydrologic linkages with floodplain sediment*

Although the six time periods studied were unequal in duration, average flow conditions were similar for most time periods, with one drier and one wetter period (Figure 4C; Table 3). The mean annual and peak discharges within the reach averaged 1.9 and 12.1 $m^3 s^{-1}$ respectively from 1935 to 2017. The period between 2012 and 2015 was a relatively dry interval with the least average number of days above both baseflow conditions and bankfull stage, the least mean and max annual volume of flow, the lowest maximum and mean peak flow, and the lowest mean and maximum total recession slope of all time periods (Table 3). Conversely, the period between 1991 and 2001 was a relatively wet interval with the highest mean duration above baseflow, the highest maximum peak flow, a relatively high total annual volume of discharge, and a relatively high number of peaks above bankfull flow conditions.

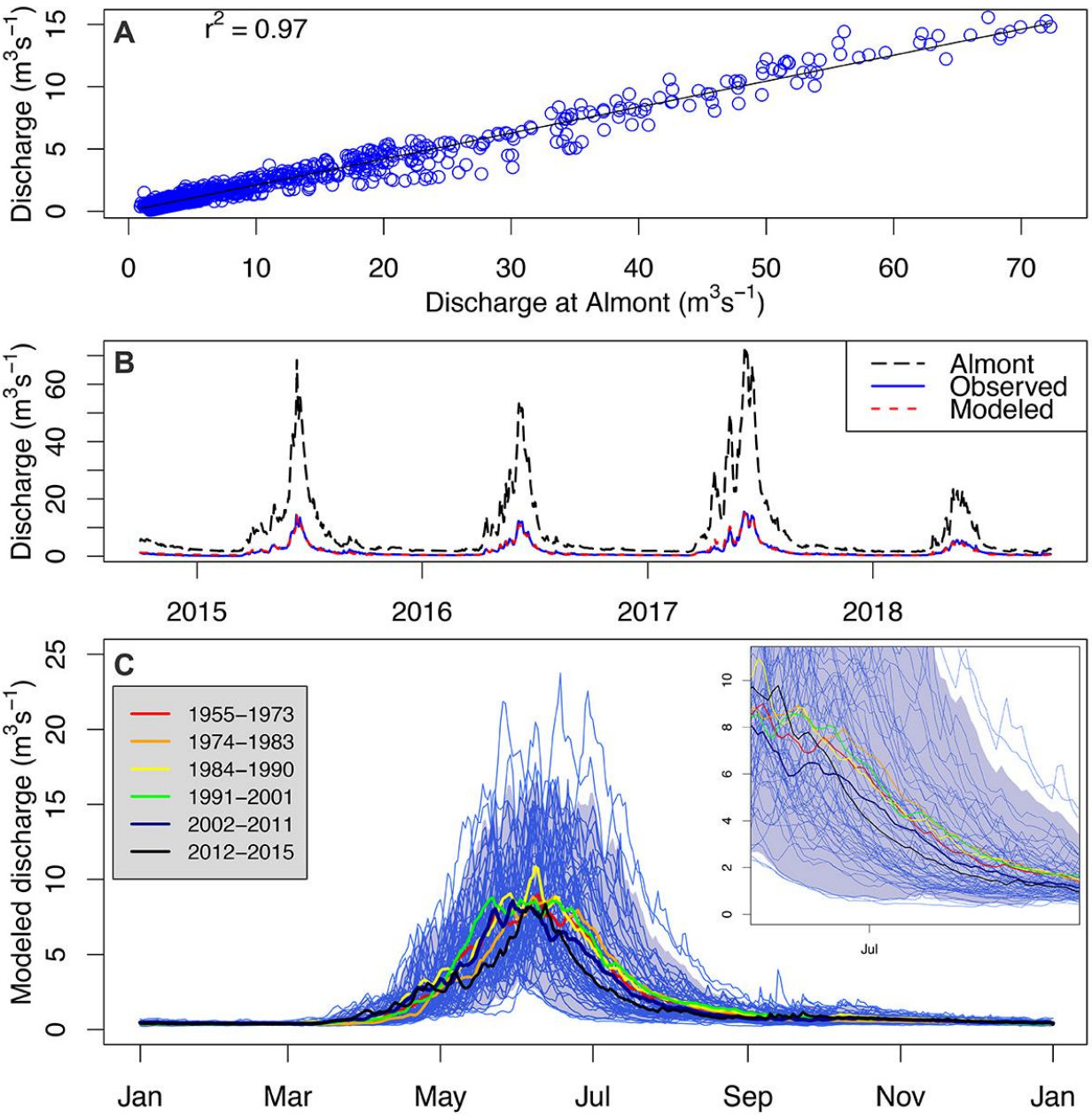


577

578 **Figure 4** Discharge at the East River study site and Almont stream gauge. (A) Linear regression
579 between measured discharge at Almont and the study site ($r^2$=0.97 ), (B) modeled discharge the
580 study site based on the regression analysis (NSE=0.97), and (C) Modeled annual hydrographs
581 for the 60-year study period (1955-2015) and an inset closeup of the hydrograph recession
582 limbs. Thin, light blue lines are annual hydrographs, the shaded blue area is the 95%
583 confidence interval, and colored lines represent mean hydrographs for the six time periods.
584

585 Multiple stepwise linear regression indicates that floodplain sediment exchange along

586 the nine study reaches during the six time intervals are explained primarily by the hydrologic

conditions and the sinuosity of the channel at the beginning of each period (Table S5). Laterally accreted area ($A_L$) with the appropriate power transformation ($\lambda$ = 0.2626) was most significantly influenced by a positive correlation with sinuosity (*P; p <0.0001*), the maximum number of days above the reference baseflow condition ($D_{base}$*; p <0.05*), the mean channel width ($w$) of the study reach (p<0.05), and the maximum bankfull recession slope ($R_{bf}$) ($r^2$ = 0.55, p < 0.1).

$$A_L^{0.26263} = -6.591 + 0.015D_{base} + 3.142P + 0.240w + 21.432\,R_{bf} \quad (2)$$

The area of floodplain erosion ($E_A$) across the nine study reaches over the 6 periods was best explained by a positive correlation with the maximum total recession slope from peak to baseflow conditions ($R_{total}$*; p<0.0001*) and sinuosity (*P; p <0.001*) and a negative correlation with the maximum time between the first and last day flow exceeded baseflow ($T_{base}$) ($r^2$ = 0.59, p < 0.05; Table S5).

$$E_A^{0.10101} = 2.058 + 5.190\,R_{total} + 0.157\,P - 0.002\,T_{base} \quad (3)$$

Examination of the hydrologic variables alone explain a much higher portion of the variability in erosion and accretion along the entire 11-km study segment. Linear regression for the entire 11-km long study segment indicated that lateral accretion was best explained by the maximum number of days flow was above bankfull stage ($r^2$ = 0.59, p = 0.074; Figure 5A). The most significant hydrologic variable for explaining the area of erosion along the 11-km long study segment was the mean slope of the hydrograph recession from peak to baseflow conditions ($r^2$ = 0.91, p = 0.003; Figure 5B).

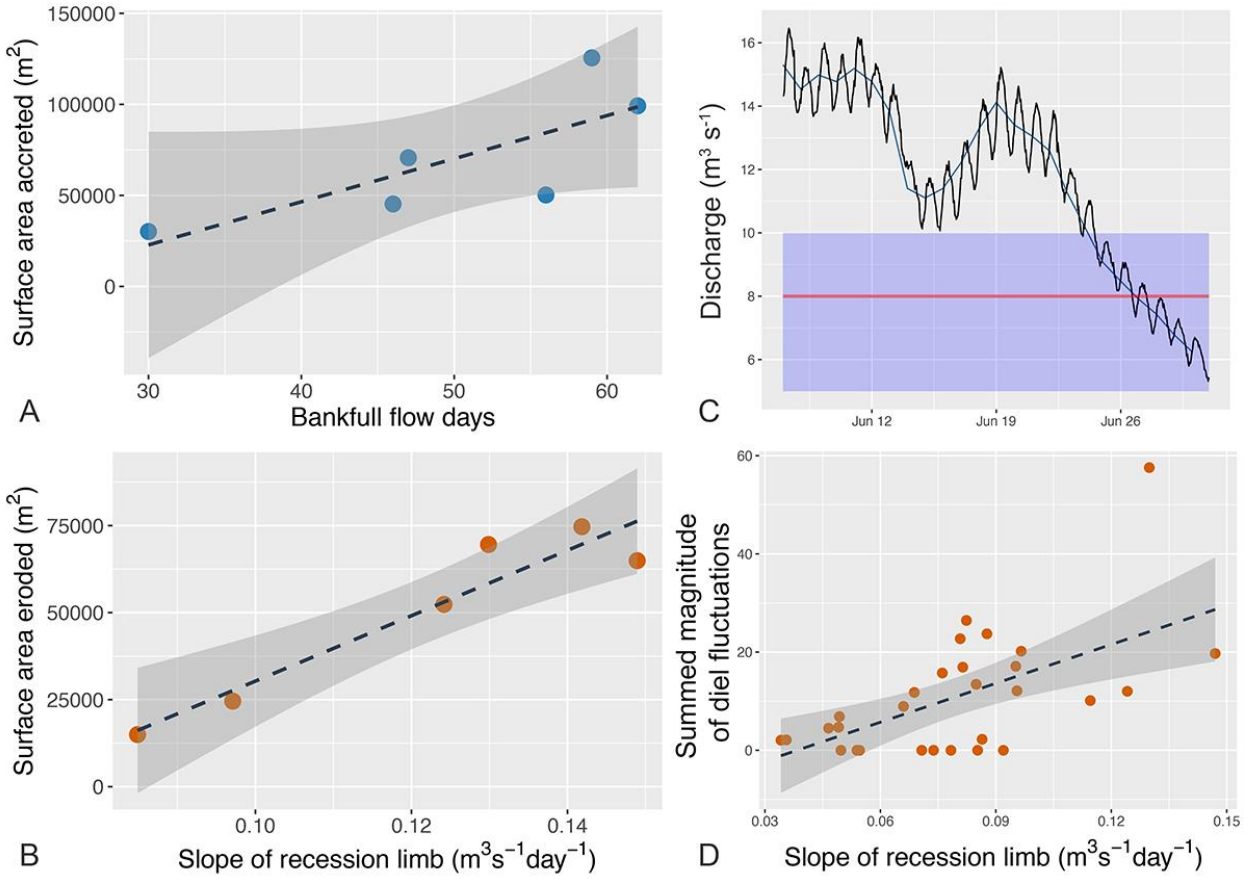


**Figure 5** Linear regression of eroded and accreted areas and diel fluctuations. Each point represents each of the six time intervals for which data from all nine study reaches are combined. (A) The number of days that flow exceeded bankfull flow conditions is a significant predictor of accreted area ($r^2$=0.59, p = 0.074) and (B) the maximum recession slope frame of the total recession slope from peak to baseflow is a significant predictor of eroded area ($r^2$=0.91, p = 0.003). (C) The recession limb of the 2017 annual hydrograph illustrates fluctuations of discharge in response to snowmelt during daily warming and cooling, which can exceed 2 $m^3$ $s^{-1}$, but do not show a strong correlation with the maximum recession slope ($r^2$=0.29) (D). In A, B, and D, the dashed lines represent the linear regression model and the gray shaded area represents the 95% confidence intervals. In C the red line represents the bankfull flow stage and the blue shaded area represents the window in which diel fluctuations were examined.

Our analysis did not show a strong correlation between the maximum recession slope and observations of associated diel fluctuations since 1988. The number, the summed magnitude, and the mean magnitude of diel fluctuations in discharge exceeding 2 $m^3s^{-1}$ within the defined window around bankfull flow ($5 < Q_{bf} < 10$ $m^3s^{-1}$) were poorly correlated with the maximum recession slope. The strongest correlation existed with the summed magnitude of diel fluctuations during each recession limb ($r^2$<0.3; Figure 5D).

## 5. Discussion

### 5.1 Floodplain volume and the sediment budget

Our floodplain fine sediment budget closed within the range of error (3920 ± 5091 $m^3$), suggesting that our approach accurately accounted for erosion and deposition. Estimates of bank erosion along cut banks and deposition along point bars are relatively robust because they were measured with calculated error from aerial imagery and based on measured depths and long-term average deposition rates. Our results linking horizontal and vertical distance from the channel with overbank deposition are consistent with published research (Asselman & Middelkoop, 1995; Hupp et al., 2008; G. Day et al., 2008). However, this approach used the total depth of sediment deposited over the 42 year period between 1973 and 2015, which does not account for deposition and subsequent erosion occurring at time scales shorter than our averaging. For these reasons, estimate of overbank sediment deposition in our sediment budget likely contain the highest uncertainty among values in our sediment budget. However, our analysis captures an average aggradation rate for each time period, effectively accounting for feedbacks between annual and decadal time scales appropriate for our analysis. Annual processes that may influence floodplain processes on decadal time scales include successful germination and establishment of riparian vegetation and cyclical patterns in channel widening and narrowing.

### 5.2 Linkages between flow duration and floodplain accretion

Potential for increased successful establishment of riparian vegetation associated with longer duration of flows and a slower recession limb of snowmelt-dominated systems (Merritt & Wohl, 2002) may explain our observed relationships between accretion and flow duration. The floodplain along our study segment of the East River is devoid of cottonwoods, but willow (Salix spp.) are present and share similar relationships between hydrochory and successful seedling

652 establishment in snowmelt-dominated systems (Karrenberg et al., 2002; Woods & Cooper,
653 2005; Cooper et al., 2006). The number of days above baseflow and days above bankfull flow
654 are the most significant hydrologic variable for lateral accretion at the 9 study reaches and the
655 11-km long study segment, respectively. Accretion could be aided by successful establishment
656 of willows along point bars during sustained high flows and observed diel fluctuations, which
657 resemble the stepped recession limb most successful at seedling establishment in Merritt &
658 Wohl (2002). Channel narrowing associated with stabilization of vegetated point bars (Friedman
659 et al., 1996; Balke et al., 2014; Caponi et al., 2019) can force flow to outer banks and encourage
660 subsequent bank erosion (Merritt & Cooper, 2000; Zen et al., 2017) and widening in cyclical
661 patterns observed on meandering rivers (Hooke, 2008; Cantelli et al., 2004). Alternating periods
662 of channel narrowing and widening have commonly been observed in the field (Hooke, 2008;
663 Cantelli et al., 2004). The period between 2012 and 2015 is the only exception in this alternating
664 pattern on the East River and may have arisen from a reduction in erosion associated with the
665 lowest maximum total recession slope in the study period.
666 Our observations show that the erosion and accretion that facilitate channel migration of
667 the East River are accompanied by channel cutoffs. Progressive increases in sinuosity of the
668 East River were truncated by 21 chute cutoffs during the study period. During that time period
669 the channel maintained a relatively stable sinuosity within each study reach and along the 11-
670 km long study segment (Table 1; Figure 3A). Many observations and most models that predict
671 channel cutoffs include only neck cutoffs, which by definition occur only after sinuosity reaches
672 a threshold that causes two river bends to meet (Howard, 1996; Hooke, 2004; Zinger et al.,
673 2011). Along a study reach of the Sacramento River exceeding 150 km, Micheli & Larsen (2011)
674 made observations similar to those we present here. The occurrence of 27 chute cutoffs helped
675 maintained an average sinuosity of 1.38 ± 0.018 (1.37-1.41) over the course of 93 years on the
676 Sacramento River. Micheli & Larsen (2011) and Hooke (2004) also hypothesize that cutoffs
677 occurred at some threshold of sinuosity and/or discharge.

678

679 5.3 *Linkages between recession slope and bank erosion*

680 Stepwise regression analysis of erosion at the nine study reaches and linear regression
681 at the 11-km long study segment suggest that the total recession slope is strongly linked to the
682 occurrence of bank erosion on the snowmelt-dominated East River. While accounting for
683 changes in sinuosity, the maximum duration between the first and last day of flow exceeding
684 baseflow conditions and the total recession slope are significant predictors in the stepwise
685 regression analysis. The total recession slope has the highest significance among variables in
686 the model ($p<0.0001$). The maximum total recession slope alone explains 91% of the variability
687 in bank erosion when considering the entire 11-km long study segment, highlighting its
688 importance on bank erosion.

689 Limited observations have previously only suggested that the recession limb slope could
690 be a significant factor in bank erosion. Although Pizzuto (1994) attributed observed bank
691 erosion on the order of 30% of the channel width in the snowmelt-dominated Powder River,
692 Montana, to elevated discharge for approximately 7 days, they also suggested a steep
693 recession limb in 1978 may have been partially responsible. Similarly, Hooke (1979) suggested
694 the recession limb slope could have played a role in observed bank erosion in a temperate
695 flashy systems, but they lacked temporal resolution necessary to examine the rate of change in
696 flow. The role of the recession limb as a mechanism for bank erosion, however, likely varies
697 substantially between the temperate stormy system examined by Hooke and snowmelt-
698 dominated discharge of the East River.

699 Observations presented here that link the total recession limb slope with erosion may
700 involve a combination of mechanisms. On the East River, we observe that high flows erode
701 underlying fluvial gravels resulting in planar cantilever failures of the fine grain upper portion of
702 the bank (Figure 1D, S1). Shifting oblique directions in subsurface hydraulic gradient observed
703 on the East River (Malenda et al., 2019), could change the magnitude and direction of confining

pressure on the outside of river bends where erosion occurs and shifts hyporheic flow toward apposing meander bends. This change in hydraulic gradient could produce a positive pore pressure along banks with a seepage face, triggering slump bank erosion (Rinaldi & Casagli, 1999; Fox et al., 2007). Although it is possible that some bank failures in the study area have been triggered by positive pore pressure, these types of failures often occur in stormy systems that experience flash floods with dramatic changes in discharge occurring over the course of a single day or several hours. Additionally, slump failures commonly occur along much higher banks (>4m) composed of heterogeneous bank material (Simon et al., 2000; Langendoen & Simon, 2008; S. S. Day et al., 2013b). Slump scarps provide evidence of occurrence, but scarps are not observed on the East River, and cantilevers failures are the primary mechanism of bank failure.

Conceptually, the loss in confining pressure explains the link between our field observations and the total recession slope in our analysis. Following undercutting of banks composed of fine sediment, the loss of supporting pressure with rapidly declining stage can result in tension cracks of undercut banks that trigger bank failure (Rinaldi & Casagli, 1999). River banks in flashy systems are likely to retain significant water following a rapid recession limb, which adds to their weight and could facilitate failure of undercut banks. The gradual decline in flow stage occurring over the course of days to weeks on the East River, and characteristic of snowmelt-dominated systems, is likely to allow silt-dominated soils to drain so that undercut banks are not as heavy. Diel fluctuations in discharge (2 to 5 $m^3s^{-1}$) during peak flow recessions on the East River near bankfull stage (~8 $m^3s^{-1}$; Figure 5C), however, could facilitate wet and even saturated conditions of river banks. These rapid changes in discharge ($Q$) equate to daily changes in flow depth ($d$) of approximately 0.02 to 0.03 m at the gauging station which has an approximate bankfull width ($w$) of 14 m. Although there is a strong correlation between total recession slope and erosion, recession slope is not correlated with diel fluctuations in our analysis (Figure 5D). Therefore our data do not draw a strong correlation

between erosion and diel fluctuations. Because the mechanistic linkage between recession slope and bank erosion in snowmelt-dominated systems in not understood, we suggest that more work is required to assess the role of diel fluctuations.

*5.4 Influence of shifting hydrologic regimes on floodplain sediment fluxes*

Linkages between hydrology and floodplain fine sediment dynamics presented here elucidate implications for snowmelt-dominated systems, particularly under shifting climatic conditions. Observed changes in snowpack, upward shifts in the rainfall-snowfall transition, rapid warming and earlier snowmelt, and increased rain-on-snow events, are altering snow-melt dominated hydrographs (Stewart et al., 2004; Clow, 2009; Kampf & Lefsky, 2016; Praskievicz, 2016; Painter et al., 2018). The coldest snowmelt regimes are likely to experience increased spring hydrograph peaks, whereas transitional snowmelt regimes may experience lower spring peaks and more winter peak events (Nijssen et al., 2001). Snowmelt-dominated hydrographs characterized by a single dominant peak with relatively little response to rain may shift to mimic characteristics of mixed rain on snow regimes that generate higher flows in the winter with possibility of multiple peaks (Hammond & Kampf, 2020). Predicted increase in the frequency or magnitude of storms (Bates et al., 2008) could make extreme floods in mountainous regions – like the one that occurred in the Colorado Front Range in 2013 – more common, which could greatly alter floodplain sediment dynamics and residence times (Sutfin & Wohl, 2019). Although observations and projections of floods do not indicate an increase in magnitude across rivers with all types of flow regimes, floods are occurring more often (Hirsch & Archfield, 2015; Mallakpour & Villarini, 2015). Higher frequency of storms has potential for more frequent floods and associated recession limbs. These changes would by definition shift otherwise predictable snowmelt dominated systems to more flashy systems with increased variability and more rapidly rising and receding limbs, but how changes could influence sediment dynamics are uncertain.

The changes in annual average snowpack and timing of snowmelt are poised to change flow durations, the slope of recession limbs, and sediment dynamics, but the direction of these changes in unknown. Let's consider a transition to flashier systems in response to consistent warming, less snowpack, and increased rain-on-snow events. Because higher flows are being distributed throughout more of the year, this type of shift is likely to result in more frequent, lower magnitude peaks with steeper recession limbs. If flow magnitude or the duration of flow is the dominant factor for erosion, as some studies suggest (Hooke, 1979; James E. Pizzuto, 1994; Langendoen & Alonso, 2008; Langendoen & Simon, 2008), the erosional response to this transition is likely to be limited. If the recession slope is the most important influence on bank erosion, as our results suggest, this transition could increase the erosional response. This erosional response paired with our findings that a positive correlation exists between floodplain accretion and the duration of overbank flow, supported by others (Asselman & Middelkoop, 1995; Hupp et al., 2008), flashier systems could limit overbank deposition while encouraging bank erosion.

## Conclusion

Our findings linking measured bank erosion and the annual snowmelt-dominated recession limb slope of the East River provide previously undocumented insight into snowmelt dominated systems, which comprise the majority of mountainous headwater streams and rivers above 40° latitude. Here we present results that integrate long-term, 60 years, of high-resolution (*1-m pixels)* remotely-sensed change analyses with extensive field observations that document deposition rates and patterns ranging from individual point bars to entire floodplain reaches over individual seasons to decades. By combining these results with detailed hydrological analysis of the East River we are able to isolate the specific component of this snowmelt-dominated hydrograph individually responsible for erosion and deposition. This analysis suggests that the floodplain sediment budget is balanced along the East River intensive study reach, which

supports the accuracy of our analysis within the calculated error. The more complex stepwise regression models indicate that channel morphometry (i.e., width, sinuosity) likely influences erosion and accretion associated with hydrologic variables along the nine study reaches. Our results linking channel accretion to the duration of flow above baseflow conditions support prior work by others regarding accretion and flow duration above a set threshold. A strong correlation between the annual recession slope and erosion along the entire study segment suggests that the faster snowmelt-dominated hydrographs decline the more bank erosion is likely to occur. These findings emphasize the importance of flow steadiness and rate of change in erosion and sediment dynamics beyond the typical peak magnitude and duration of bankfull discharge. Thus, observed and future changes in hydrologic flow regime with changes in snowpack, snowmelt, and the rain-snow transition are likely to drive changes in the relative balance of floodplain erosion and deposition in mountainous headwaters systems. Similar changes in floodplain sediment fluxes may also occur in northern high-latitude rivers characterized by snowmelt dominated hydrographs. These changes will alter river dynamics, sediment, carbon, and nutrient fluxes, and potentially negatively impact infrastructure within river corridors.

**Acknowledgement:**

This work was funded by an Early Career award to Rowland by the Subsurface Biogeochemical Research Programs within the U.S. Department of Energy Office of Science, Biological and Environmental Research Program. This material is partially based upon work supported through the Lawrence Berkeley National Laboratory's Watershed Function Scientific Focus Area (operated by the University of California) funded by the U.S. Department of Energy (DOE), Office of Science, Office of Biological and Environmental Research contract DE-AC02-05CH11231. We thank the Rocky Mountain Biological Research Station for their support and Meghan King and Anastasia Piliouras for their assistance in the field. All data used for this study are provided in the manuscript and Supporting Information, or cited and listed in the references.

807 The R code used to extract hydrologic parameters are provided as Supporting Information as
808 cited in the text. This manuscript was greatly improved by comments from four anonymous
809 reviewers and the associate editor.
810
811 **References**

812 Adam, J. C., Hamlet, A. F., & Lettenmaier, D. P. (2009). Implications of global climate change
813 for snowmelt hydrology in the twenty-first century. *Hydrological Processes*, *23*(7), 962–
814 972. https://doi.org/10.1002/hyp.7201
815 Andrews, E. D. (1984). Bed-material entrainment and hydraulic geometry of gravel-bed rivers in
816 Colorado. *GSA Bulletin*, *95*(3), 371–378. https://doi.org/10.1130/0016-
817 7606(1984)95<371:BEAHGO>2.0.CO;2
818 Asselman, N. E. M., & Middelkoop, H. (1995). Floodplain sedimentation: Quantities, patterns
819 and processes. *Earth Surface Processes and Landforms*, *20*(6), 481–499.
820 https://doi.org/10.1002/esp.3290200602
821 Balke, T., Herman, P. M. J., & Bouma, T. J. (2014). Critical transitions in disturbance-driven
822 ecosystems: identifying Windows of Opportunity for recovery. *Journal of Ecology*,
823 *102*(3), 700–708. https://doi.org/10.1111/1365-2745.12241
824 Bates, B., Kundzewicz, Z. W., Wu, S., Burkett, V., Doell, P., Gwary, D., et al. (2008). *Climate*
825 *Change and Water. Technical Paper of the Intergovernmental Panel on Climate Change*.
826 Begin, Z. B. (1981). Stream Curvature and Bank Erosion: A Model Based on the Momentum
827 Equation. *The Journal of Geology*, *89*(4), 497–504. https://doi.org/10.1086/628610
828 Benjankar, R., Burke, M., Yager, E., Tonina, D., Egger, G., Rood, S. B., & Merz, N. (2014).
829 Development of a spatially-distributed hydroecological model to simulate cottonwood

seedling recruitment along rivers. *Journal of Environmental Management*, *145*, 277–288. https://doi.org/10.1016/j.jenvman.2014.06.027

Cantelli, A., Paola, C., & Parker, G. (2004). Experiments on upstream-migrating erosional narrowing and widening of an incisional channel caused by dam removal. *Water Resources Research*, *40*(3). https://doi.org/10.1029/2003WR002940

Caponi, F., Koch, A., Bertoldi, W., Vetsch, D. F., & Siviglia, A. (2019). When Does Vegetation Establish on Gravel Bars? Observations and Modeling in the Alpine Rhine River. *Frontiers in Environmental Science*, *7*. https://doi.org/10.3389/fenvs.2019.00124

Carroll, R., & Williams, K. (2019). Discharge data collected within the East River for the Lawrence Berkeley National Laboratory Watershed Function Science Focus Area (water years 2015-2018), Watershed Function SFA. *EES-DIVE: Deep Insight for Earth Science*. http://dx.doi.org/10.21952/WTR/1495380

Clow, D. W. (2009). Changes in the Timing of Snowmelt and Streamflow in Colorado: A Response to Recent Warming. *Journal of Climate*, *23*(9), 2293–2306. https://doi.org/10.1175/2009JCLI2951.1

Cooper, D. J., Merritt, D. M., Andersen, D. C., & Chimner, R. A. (1999). Factors controlling the establishment of Fremont cottonwood seedlings on the Upper Green River, USA. *Regulated Rivers: Research & Management*, *15*(5), 419–440. https://doi.org/10.1002/(SICI)1099-1646(199909/10)15:5<419::AID-RRR555>3.0.CO;2-Y

Cooper, D. J., Dickens, J., Hobbs, N. T., Christensen, L., & Landrum, L. (2006). Hydrologic, geomorphic and climatic processes controlling willow establishment in a montane ecosystem. *Hydrological Processes*, *20*(8), 1845–1864. https://doi.org/10.1002/hyp.5965

Darby, S. E., Rinaldi, M., & Dapporto, S. (2007). Coupled simulations of fluvial erosion and mass wasting for cohesive river banks. *Journal of Geophysical Research: Earth Surface, 112*(F3). https://doi.org/10.1029/2006JF000722

Day, G., Dietrich, W. E., Rowland, J. C., & Marshall, A. (2008). The depositional web on the floodplain of the Fly River, Papua New Guinea. *Journal of Geophysical Research: Earth Surface, 113*. https://doi.org/10.1029/2006JF000622@10.1002/(ISSN)2169-9011.PAPUA1

Day, S. S., Gran, K. B., Belmont, P., & Wawrzyniec, T. (2013a). Measuring bluff erosion part 1: terrestrial laser scanning methods for change detection. *Earth Surface Processes and Landforms*, *38*(10), 1055–1067. https://doi.org/10.1002/esp.3353

Day, S. S., Gran, K. B., Belmont, P., & Wawrzyniec, T. (2013b). Measuring bluff erosion part 2: pairing aerial photographs and terrestrial laser scanning to create a watershed scale sediment budget. *Earth Surface Processes and Landforms*, *38*(10), 1068–1082. https://doi.org/10.1002/esp.3359

Donovan, M., Belmont, P., Notebaert, B., Coombs, T., Larson, P., & Souffront, M. (2019). Accounting for uncertainty in remotely-sensed measurements of river planform change. *Earth-Science Reviews*, *193*, 220–236. https://doi.org/10.1016/j.earscirev.2019.04.009

Dormann, C. F., Elith, J., Bacher, S., Buchmann, C., Carl, G., Carré, G., et al. (2013). Collinearity: a review of methods to deal with it and a simulation study evaluating their performance. *Ecography*, *36*(1), 27–46. https://doi.org/10.1111/j.1600-0587.2012.07348.x

Fisher, G. B., Bookhagen, B., & Amos, C. B. (2013). Channel planform geometry and slopes from freely available high-spatial resolution imagery and DEM fusion: Implications for

channel width scalings, erosion proxies, and fluvial signatures in tectonically active landscapes. *Geomorphology*, *194*, 46–56. https://doi.org/10.1016/j.geomorph.2013.04.011

Fox, G. A., Wilson, G. V., Simon, A., Langendoen, E. J., Akay, O., & Fuchs, J. W. (2007). Measuring streambank erosion due to ground water seepage: correlation to bank pore water pressure, precipitation and stream stage. *Earth Surface Processes and Landforms*, *32*(10), 1558–1573. https://doi.org/10.1002/esp.1490

Friedman, J. M., Osterkamp, W. R., & Lewis, W. M. (1996). Channel Narrowing and Vegetation Development Following a Great Plains Flood. *Ecology*, *77*(7), 2167–2181. https://doi.org/10.2307/2265710

Furbish, D. J. (1991). Spatial autoregressive structure in meander evolution. *GSA Bulletin*, *103*(12), 1576–1589. https://doi.org/10.1130/0016-7606(1991)103<1576:SASIME>2.3.CO;2

Gaskill, D. L., Mutschler, F. E., Kramer, J. H., Thomas, J. A., & Zahony, S. G. (1991). Geologic map of the Gothic quadrangle, Gunnison County, Colorado. Geologic Quadrangle Map GQ-1689, sale 1:24,000, Gunnison, Colorado: U.S. Geological Survey.

Grams, P. E., Dean, D. J., Walker, A. E., Kasprak, A., & Schmidt, J. C. (2020). The roles of flood magnitude and duration in controlling channel width and complexity on the Green River in Canyonlands, Utah, USA. *Geomorphology*, *371*, 107438. https://doi.org/10.1016/j.geomorph.2020.107438

Güneralp, İ., & Rhoads, B. L. (2009). Empirical analysis of the planform curvature-migration relation of meandering rivers. *Water Resources Research*, *45*(9), W09424. https://doi.org/10.1029/2008WR007533

Gurnell, A. M. (1997). Channel change on the River Dee meanders, 1946–1992, from the analysis of air photographs. *Regulated Rivers: Research & Management*, *13*(1), 13–26. https://doi.org/10.1002/(SICI)1099-1646(199701)13:1<13::AID-RRR420>3.0.CO;2-W

Hammond, J. C., & Kampf, S. K. (2020). Subannual Streamflow Responses to Rainfall and Snowmelt Inputs in Snow-Dominated Watersheds of the Western United States. *Water Resources Research*, *56*(4), e2019WR026132. https://doi.org/10.1029/2019WR026132

Hirsch, R. M., & Archfield, S. A. (2015). Flood trends: Not higher but more often. *Nature Climate Change*, *5*(3), 198–199. https://doi.org/10.1038/nclimate2551

Hooke, J. M. (1979). An analysis of the processes of river bank erosion. *Journal of Hydrology*, *42*(1), 39–62. https://doi.org/10.1016/0022-1694(79)90005-2

Hooke, J. M. (1980). Magnitude and distribution of rates of river bank erosion. *Earth Surface Processes*, *5*(2), 143–157. https://doi.org/10.1002/esp.3760050205

Hooke, J. M. (2004). Cutoffs galore!: occurrence and causes of multiple cutoffs on a meandering river. *Geomorphology*, *61*(3), 225–238. https://doi.org/10.1016/j.geomorph.2003.12.006

Hooke, J. M. (2007). Spatial variability, mechanisms and propagation of change in an active meandering river. *Geomorphology*, *84*(3), 277–296. https://doi.org/10.1016/j.geomorph.2006.06.005

Hooke, J. M. (2008). Temporal variations in fluvial processes on an active meandering river over a 20-year period. *Geomorphology*, *100*(1), 3–13. https://doi.org/10.1016/j.geomorph.2007.04.034

Howard, A. D. (1996). Modeling Channel Evolution and Floodplain Morphology. *Floodplain Processes*, 15–62.

Hupp, C. R., Demas, C. R., Kroes, D. E., Day, R. H., & Doyle, T. W. (2008). Recent sedimentation patterns within the central Atchafalaya Basin, Louisiana. *Wetlands*, *28*(1), 125–140. https://doi.org/10.1672/06-132.1

James E. Pizzuto. (1994). Channel adjustments to changing discharges, Powder River, Montana. *GSA Bulletin*, *106*(11), 1494–1501. https://doi.org/10.1130/0016-7606(1994)106<1494:CATCDP>2.3.CO;2

Kampf, S. K., & Lefsky, M. A. (2016). Transition of dominant peak flow source from snowmelt to rainfall along the Colorado Front Range: Historical patterns, trends, and lessons from the 2013 Colorado Front Range floods. *Water Resources Research*, *52*(1), 407–422. https://doi.org/10.1002/2015WR017784

Karrenberg, S., Edwards, P. J., & Kollmann, J. (2002). The life history of Salicaceae living in the active zone of floodplains. *Freshwater Biology*, *47*(4), 733–748. https://doi.org/10.1046/j.1365-2427.2002.00894.x

Langendoen, E. J., & Alonso, C. V. (2008). Modeling the Evolution of Incised Streams: I. Model Formulation and Validation of Flow and Streambed Evolution Components. *Journal of Hydraulic Engineering*, *134*(6), 749–762. https://doi.org/10.1061/(ASCE)0733-9429(2008)134:6(749)

Langendoen, E. J., & Simon, A. (2008). Modeling the Evolution of Incised Streams. II: Streambank Erosion. *Journal of Hydraulic Engineering*, *134*(7), 905–915. https://doi.org/10.1061/(ASCE)0733-9429(2008)134:7(905)

Lenhart, C. F., Titov, M. L., Ulrich, J. S., Nieber, J. L., & Suppes, B. J. (2013). The Role of Hydrologic Alteration and Riparian Vegetation Dynamics in Channel Evolution along the

Lower Minnesota River. *Transactions of the American Society of Agricultural and Biological Engineers*, *56*(2), 549–561.

Lininger, K. B., Wohl, E., & Rose, J. R. (2018). Geomorphic Controls on Floodplain Soil Organic Carbon in the Yukon Flats, Interior Alaska, From Reach to River Basin Scales. *Water Resources Research*, *54*(3), 1934–1951. https://doi.org/10.1002/2017WR022042

Lininger, K. B., Wohl, E., Rose, J. R., & Leisz, S. J. (2019). Significant Floodplain Soil Organic Carbon Storage Along a Large High-Latitude River and its Tributaries. *Geophysical Research Letters*, *46*(4), 2121–2129. https://doi.org/10.1029/2018GL080996

Mahoney, J. M., & Rood, S. B. (1998). Streamflow requirements for cottonwood seedling recruitment—An integrative model. *Wetlands*, *18*(4), 634–645. https://doi.org/10.1007/BF03161678

Malenda, H. f., Sutfin, N. a., Guryan, G., Stauffer, S., Rowland, J. c., Williams, K. h., & Singha, K. (2019). From Grain to Floodplain: Evaluating heterogeneity of floodplain hydrostatigraphy using sedimentology, geophysics, and remote sensing. *Earth Surface Processes and Landforms*, *0*(0). https://doi.org/10.1002/esp.4613

Mallakpour, I., & Villarini, G. (2015). The changing nature of flooding across the central United States. *Nature Climate Change*, *5*(3), 250–254. https://doi.org/10.1038/nclimate2516

McClelland, J. W., Holmes, R. M., Dunton, K. H., & Macdonald, R. W. (2012). The Arctic Ocean Estuary. *Estuaries and Coasts*, *35*(2), 353–368. https://doi.org/10.1007/s12237-010-9357-3

McFeeters, S. K. (1996). The use of the Normalized Difference Water Index (NDWI) in the delineation of open water features. *International Journal of Remote Sensing*, *17*(7), 1425–1432. https://doi.org/10.1080/01431169608948714

966 Merritt, D. M., & Cooper, D. J. (2000). Riparian vegetation and channel change in response to
967 river regulation: a comparative study of regulated and unregulated streams in the Green
968 River Basin, USA. *Regulated Rivers: Research & Management*, *16*(6), 543–564.
969 https://doi.org/10.1002/1099-1646(200011/12)16:6<543::AID-RRR590>3.0.CO;2-N
970 Merritt, D. M., & Wohl, E. E. (2002). Processes Governing Hydrochory Along Rivers:
971 Hydraulics, Hydrology, and Dispersal Phenology. *Ecological Applications*, *12*(4), 1071–
972 1087. https://doi.org/10.1890/1051-0761(2002)012[1071:PGHARH]2.0.CO;2
973 Metzger, T. L., Pizzuto, J. E., Trampush, S. M., Friedman, J. M., & Schook, D. M. (2020).
974 Event-scale floodplain accretion revealed through tree-ring analysis of buried plains
975 cottonwoods, Powder River, MT, USA. *Earth Surface Processes and Landforms*, *45*(2),
976 345–360. https://doi.org/10.1002/esp.4734
977 Micheli, E. R., & Kirchner, J. W. (2002a). Effects of wet meadow riparian vegetation on
978 streambank erosion. 1. Remote sensing measurements of streambank migration and
979 erodibility. *Earth Surface Processes and Landforms*, *27*(6), 627–639.
980 https://doi.org/10.1002/esp.338
981 Micheli, E. R., & Kirchner, J. W. (2002b). Effects of wet meadow riparian vegetation on
982 streambank erosion. 2. Measurements of vegetated bank strength and consequences for
983 failure mechanics. *Earth Surface Processes and Landforms*, *27*(7), 687–697.
984 https://doi.org/10.1002/esp.340
985 Micheli, E. R., & Larsen, E. W. (2011). River channel cutoff dynamics, Sacramento River,
986 California, USA. *River Research and Applications*, *27*(3), 328–344.
987 https://doi.org/10.1002/rra.1360

Middelkoop, H., Daamen, K., Gellens, D., Grabs, W., Kwadijk, J. C. J., Lang, H., et al. (2001). Impact of Climate Change on Hydrological Regimes and Water Resources Management in the Rhine Basin. *Climatic Change*, *49*(1), 105–128. https://doi.org/10.1023/A:1010784727448

Mount, N., & Louis, J. (2005). Estimation and propagation of error in measurements of river channel movement from aerial imagery. *Earth Surface Processes and Landforms*, *30*(5), 635–643. https://doi.org/10.1002/esp.1172

Nanson Gerald C., & Hickin Edward J. (1983). Channel Migration and Incision on the Beatton River. *Journal of Hydraulic Engineering*, *109*(3), 327–337. https://doi.org/10.1061/(ASCE)0733-9429(1983)109:3(327)

Nijssen, B., O'Donnell, G. M., Hamlet, A. F., & Lettenmaier, D. P. (2001). Hydrologic Sensitivity of Global Rivers to Climate Change. *Climatic Change*, *50*(1), 143–175. https://doi.org/10.1023/A:1010616428763

Nilsson, C., Brown, R. L., Jansson, R., & Merritt, D. M. (2010). The role of hydrochory in structuring riparian and wetland vegetation. *Biological Reviews*, *85*(4), 837–858. https://doi.org/10.1111/j.1469-185X.2010.00129.x

Painter, T. H., Skiles, S. M., Deems, J. S., Brandt, W. T., & Dozier, J. (2018). Variation in Rising Limb of Colorado River Snowmelt Runoff Hydrograph Controlled by Dust Radiative Forcing in Snow. *Geophysical Research Letters*, *45*(2), 797–808. https://doi.org/10.1002/2017GL075826

Parker, G., Sawai, K., & Ikeda, S. (1982). Bend theory of river meanders. Part 2. Nonlinear deformation of finite-amplitude bends. *Journal of Fluid Mechanics*, *115*, 303–314. https://doi.org/10.1017/S0022112082000767

Partheniades, E. (1965). Erosion and Deposition of Cohesive Soils. *Journal of the Hydraulics Division*, *91*(1), 105–139.

Pitlick, J., & Steeter, M. M. V. (1998). Geomorphology and endangered fish habitats of the upper Colorado River: 2. Linking sediment transport to habitat maintenance. *Water Resources Research*, *34*(2), 303–316. https://doi.org/10.1029/97WR02684

Pizzuto, J. E., & Meckelnburg, T. S. (1989). Evaluation of a linear bank erosion equation. *Water Resources Research*, *25*(5), 1005–1013. https://doi.org/10.1029/WR025i005p01005

Pizzuto, James E. (1994). Channel adjustments to changing discharges, Powder River, Montana. *GSA Bulletin*, *106*(11), 1494–1501. https://doi.org/10.1130/0016-7606(1994)106<1494:CATCDP>2.3.CO;2

Poff, N. LeRoy, Allan, J. D., Bain, M. B., Karr, J. R., Prestegaard, K. L., Richter, B. D., et al. (1997). The Natural Flow Regime. *BioScience*, *47*(11), 769–784. https://doi.org/10.2307/1313099

Poff, N. Leroy, Richter, B. D., Arthington, A. H., Bunn, S. E., Naiman, R. J., Kendy, E., et al. (2010). The ecological limits of hydrologic alteration (ELOHA): a new framework for developing regional environmental flow standards. *Freshwater Biology*, *55*(1), 147–170. https://doi.org/10.1111/j.1365-2427.2009.02204.x

Praskievicz, S. (2016). Impacts of Projected Climate Changes on Streamflow and Sediment Transport for Three Snowmelt-Dominated Rivers in the Interior Pacific Northwest. *River Research and Applications*, *32*(1), 4–17. https://doi.org/10.1002/rra.2841

Richard, G. A., Julien, P. Y., & Baird, D. C. (2005). Statistical analysis of lateral migration of the Rio Grande, New Mexico. *Geomorphology*, *71*(1), 139–155. https://doi.org/10.1016/j.geomorph.2004.07.013

1034 Rinaldi, M., & Casagli, N. (1999). Stability of streambanks formed in partially saturated soils
1035 and effects of negative pore water pressures: the Sieve River (Italy). *Geomorphology*,
1036 *26*(4), 253–277. https://doi.org/10.1016/S0169-555X(98)00069-5
1037 Rowland, J. C., & Stauffer, S. (2020). *Classified channel masks of the East River, Colorado,*
1038 *U.S.A and areas of floodplain erosion and accretion ranging from 1955 to 2015*.
1039 Environmental System Science Data Infrastructure for a Virtual Ecosystem (ESS-DIVE)
1040 (United States); Incorporating the Hydrological Controls on Carbon Cycling in
1041 Floodplain Ecosystems into Earth System Models (ESMs).
1042 https://doi.org/10.15485/1642909
1043 Rowland, J. C., Shelef, E., Pope, P. A., Muss, J., Gangodagamage, C., Brumby, S. P., & Wilson,
1044 C. J. (2016). A morphology independent methodology for quantifying planview river
1045 change and characteristics from remotely sensed imagery. *Remote Sensing of*
1046 *Environment*, *184*, 212–228. https://doi.org/10.1016/j.rse.2016.07.005
1047 Schneider, C., Laizé, C. L. R., Acreman, M. C., & Flörke, M. (2013). How will climate change
1048 modify river flow regimes in Europe? *Hydrology and Earth System Sciences*, *17*(1), 325–
1049 339. https://doi.org/10.5194/hess-17-325-2013
1050 Schook, D. M., Rathburn, S. L., Friedman, J. M., & Wolf, J. M. (2017). A 184-year record of
1051 river meander migration from tree rings, aerial imagery, and cross sections.
1052 *Geomorphology*, *293*, 227–239. https://doi.org/10.1016/j.geomorph.2017.06.001
1053 Schwenk, J., Khandelwal, A., Fratkin, M., Kumar, V., & Foufoula-Georgiou, E. (2017). High
1054 spatiotemporal resolution of river planform dynamics from Landsat: The RivMAP
1055 toolbox and results from the Ucayali River. *Earth and Space Science*, *4*(2),
1056 2016EA000196. https://doi.org/10.1002/2016EA000196

Simon, A., Curini, A., Darby, S. E., & Langendoen, E. J. (2000). Bank and near-bank processes in an incised channel. *Geomorphology*, *35*(3), 193–217. https://doi.org/10.1016/S0169-555X(00)00036-2

Simon, A., Thomas, R. E., Curini, A., & Shields, F. D. (2002). Case Study: Channel Stability of the Missouri River, Eastern Montana. *Journal of Hydraulic Engineering*, *128*(10), 880–890. https://doi.org/10.1061/(ASCE)0733-9429(2002)128:10(880)

Stewart, I. T., Cayan, D. R., & Dettinger, M. D. (2004). Changes in Snowmelt Runoff Timing in Western North America under a `Business as Usual' Climate Change Scenario. *Climatic Change*, *62*(1), 217–232. https://doi.org/10.1023/B:CLIM.0000013702.22656.e8

Sutfin, N. A., & Rowland, J. C. (2019). Depth and elevation of floodplain fine sediment along the East River near Crested Butte, Colorado measured in 2016 and 2017. Incorporating the Hydrological Controls on Carbon Cycling in Floodplain Ecosystems into Earth System Models (ESMs). *ESS-Dive: Deep Insight for Earth Science Data*. https://doi.org/doi:10.15485/1574502

Sutfin, N. A., & Wohl, E. (2017). Substantial soil organic carbon retention along floodplains of mountain streams. *Journal of Geophysical Research: Earth Surface*, *122*(7), 1325–1338. https://doi.org/10.1002/2016JF004004

Sutfin, N. A., & Wohl, E. (2019). Elevational differences in hydrogeomorphic disturbance regime influence sediment residence times within mountain river corridors. *Nature Communications*, *10*(1), 2221. https://doi.org/10.1038/s41467-019-09864-w

Sutfin, N. A., Wohl, E. E., & Dwire, K. A. (2016). Banking carbon: a review of organic carbon storage and physical factors influencing retention in floodplains and riparian ecosystems. *Earth Surface Processes and Landforms*, *41*(1), 38–60. https://doi.org/10.1002/esp.3857

Sylvester, Z., Durkin, P., & Covault, J. A. (2019). High curvatures drive river meandering. *Geology*, *47*(3), 263–266. https://doi.org/10.1130/G45608.1

Theobald, D. M., Gosnell, H., & Riebsame, W. E. (1996). Land Use and Landscape Change in the Colorado Mountains II: A Case Study of the East River Valley. *Mountain Research and Development*, *16*(4), 407–418. https://doi.org/10.2307/3673990

Thorne, C. R., & Tovey, N. K. (1981). Stability of composite river banks. *Earth Surface Processes and Landforms*, *6*(5), 469–484. https://doi.org/10.1002/esp.3290060507

Wainwright, H., & Williams, K. (2017). *LiDAR collection in August 2015 over the East River Watershed, Colorado, USA*. Lawrence Berkeley National Lab. (LBNL), Berkeley, CA (United States). https://doi.org/10.21952/WTR/1412542

Wohl, E., Bledsoe, B. P., Jacobson, R. B., Poff, N. L., Rathburn, S. L., Walters, D. M., & Wilcox, A. C. (2015). The Natural Sediment Regime in Rivers: Broadening the Foundation for Ecosystem Management. *BioScience*, *65*(4), 358–371. https://doi.org/10.1093/biosci/biv002

Wolf, E. C., Cooper, D. J., & Hobbs, N. T. (2007). Hydrologic Regime and Herbivory Stabilize an Alternative State in Yellowstone National Park. *Ecological Applications*, *17*(6), 1572–1587. https://doi.org/10.1890/06-2042.1

Wolman, M. G. (1959). Factors Influencing Erosion of a Cohesive River Bank. *American Journal of Science*, *257*(3), 204–216. https://doi.org/10.2475/ajs.257.3.204

Woods, S. W., & Cooper, D. J. (2005). Hydrologic Factors Affecting Initial Willow Seedling Establishment along a Subalpine Stream, Colorado, U.S.A. *Arctic, Antarctic, and Alpine Research*, *37*(4), 636–643. https://doi.org/10.1657/1523-0430(2005)037[0636:HFAIWS]2.0.CO;2

Zen, S., Gurnell, A. M., Zolezzi, G., & Surian, N. (2017). Exploring the role of trees in the evolution of meander bends: The Tagliamento River, Italy. *Water Resources Research*, *53*(7), 5943–5962. https://doi.org/10.1002/2017WR020561

Zinger, J. A., Rhoads, B. L., & Best, J. L. (2011). Extreme sediment pulses generated by bend cutoffs along a large meandering river. *Nature Geoscience*, *4*(10), 675–678. https://doi.org/10.1038/ngeo1260